# Significant source of secondary aerosol: formation from gasoline evaporative emissions in the presence of $SO_2$ and $NH_3$

**Tianzeng Chen[1, 3, a], Yongchun Liu[2, a], Qingxin Ma[1, 3, 4, *], Biwu Chu[1, 3, 4], Peng Zhang [1], Changgeng Liu[1], Jun Liu[1, 3], Hong He[1, 3, 4, *]**

[1] State Key Joint Laboratory of Environment Simulation and Pollution Control, Research Center for Eco-Environmental Sciences, Chinese Academy of Sciences, Beijing 100085, China

[2] Beijing Advanced Innovation center for Soft Matter Science and Engineering, Beijing University of Chemical Technology, Beijing 100029, China

[3] University of Chinese Academy of Sciences, Beijing 100049, China

[4] Center for Excellence in Regional Atmospheric Environment, Institute of Urban Environment, Chinese Academy of Sciences, Xiamen 361021, China

[a] These authors contributed equally to this work and should be considered as co-first authors

*Corresponding authors:* qxma@rcees.ac.cn (Qingxin Ma), and honghe@rcees.ac.cn (Hong He)

# Abstract

Gasoline evaporative emissions have become an important anthropogenic source of urban atmospheric volatile organic compounds (VOCs) and secondary organic aerosol (SOA). These emissions have a significant impact on regional air quality, especially in China where car ownership is growing rapidly. However, the contribution of evaporative emissions on the secondary aerosol (SA) is not clear in air pollution complex in which high concentration of $SO_2$ and $NH_3$ was present. In this study, the effects of $SO_2$ and $NH_3$ on SA formation from unburned gasoline vapors were investigated in a 30 $m^3$ indoor smog chamber. It was found that increase in $SO_2$ and $NH_3$ concentrations (0−151 ppb and 0−200 ppb, respectively) could promote linearly the formation of SA, which could be enhanced by a factor of 1.6−2.6 and 2.0−2.5, respectively. Sulfate was most sensitive to the $SO_2$ concentration, followed by organic aerosol, which was due not only to the acid catalytic effect, but also related to the formation of organic sulfur-containing compounds. In the case of increasing $NH_3$ concentration, ammonium nitrate increased more significantly than organic aerosol, and nitrogen-containing organics were also enhanced, as revealed by the results of positive matrix factorization (PMF) analysis. New particle formation (NPF) and particle size growth were also significantly enhanced in the presence of $SO_2$ and $NH_3$. This work indicates that gasoline evaporative emissions will be a significant source of SA, especially in the presence of high concentrations of $SO_2$ and $NH_3$. Meanwhile, these emissions might also be a potential source of sulfur- and nitrogen-containing organics. Our work provides a scientific basis for the synergistic emission reduction of secondary aerosol precursors, including $NO_x$, $SO_2$, $NH_3$ and particularly VOCs, to mitigate PM pollution in China.



# Keywords

36 Secondary inorganic aerosol; Secondary organic aerosol; Sulfur dioxide; Ammonia; Sulfur-
37 containing organics; Nitrogen-containing organics

# 1 Introduction

Many areas in China such as the Beijing - Tianjin - Hebei region (BTH), Yangtze River Delta (YRD), Sichuan Basin and Pearl River Delta (PRD) are suffering from severe haze events (Li et al., 2017; Sun et al., 2016; Shen et al., 2015; He et al., 2014; Huang et al., 2014; Guo et al., 2014; Tan et al., 2009). Haze pollution has attracted widespread attention in recent years because of its adverse effects on human health, climate change and visibility (Thalman et al., 2017; Davidson et al., 2005; Pöschl, 2005).

During the haze events, high concentrations of $SO_2$, $NH_3$, and volatile organic compounds (VOCs) have always been observed (Zou et al., 2015; Liu et al., 2013; Meng et al., 2011; Yang et al., 2009), which are the precursors of secondary aerosol. Although the emission of $SO_2$ has decreased continuously since 2005 (Lu et al., 2010), China is still the largest contributor of $SO_2$ emissions in the world, mainly owing to the great demand for coal combustion (Bauduin et al., 2016). Also, high concentrations of $SO_2$ of more than 100 ppb (parts per billion) have been observed in northern China, especially during the heating period (Hou et al., 2016; Tong et al., 2016; Yang et al., 2009). As for atmospheric $NH_3$, as an alkaline inorganic gas, its main emission source is agricultural practices in China (Zhang et al., 2018; Fu et al., 2015). Vehicles equipped with three-way catalytic converters also contributes to $NH_3$ emission in the urban areas (Sun et al., 2017). Sometimes, high concentrations of $NH_3$ of up to 100 ppb have been observed in Beijing, China (Ianniello et al., 2010), which mainly derived from the regionally transportation of agricultural activity and fertilizer use, while could not exclude the influence by traffic emissions at local Beijing (Pan et al., 2016; Kang et al., 2016). With respect to VOCs, aromatics from anthropogenic sources (especially vehicle-related sources in urban areas) are critical secondary organic aerosol (SOA) precursors (Liu et al., 2015a; Gordon et al., 2014; Platt et al., 2013; Calvert et al., 2002). These aromatics could react with oxidants (e.g., $O_3$, OH, and $NO_3$ radicals), and undergo multi-step oxidative processes to form multifunctional products, which have

sufficiently low volatility to contribute to SOA via gas-particle partitioning (Hallquist et al., 2009; Atkinson and Arey, 2003).

Researches have shown that secondary aerosol (SA) makes a significant contribution (30−77%) to $PM_{2.5}$ (particles with diameter less than 2.5 μm) during the severe haze events in China (Huang et al., 2014; Guo et al., 2014; Jimenez et al., 2009). However, there still exists a significant gap between the predicted SA derived from the current atmospheric quality models and that observed in field observations (Zhao et al., 2018; Yang et al., 2018; Zheng et al., 2015). Therefore, considering the characteristics of complex pollution in China, it is crucial to study the synergistic effects of $SO_2$ and $NH_3$ on the formation of SA, which have been considered an important potential source of SA formation (Zhao et al., 2018; Chu et al., 2016; Liu et al., 2016; Santiago et al., 2012; Na et al., 2007).

A few studies have focused on the influence of $SO_2$ or $NH_3$ on SA formation. Jang and Kamens (2001) first reported the acid-catalytical effect of acidic $H_2SO_4$ on the oxidation of atmospheric carbonyls. And the promotion effect of $SO_2$ were further found on the SA formation from typical biogenic (e.g., isoprene and α-pinene) (Lin et al., 2013; Jaoui et al., 2008; Kleindienst et al., 2006; Edney et al., 2005) and anthropogenic (e.g., toluene, o-xylene, 1,3,5-trimethylbenzene, and gasoline vehicle exhaust) precursors (Chu et al., 2016; Liu et al., 2016; Santiago et al., 2012) through acid-catalyzed heterogeneous reactions (Jang et al., 2002; Jang et al., 2003a, b; Czoschke et al., 2003), which promote the reactive uptake process of organic species or enhance the formation of high-molecular-weight compounds (Liggio and Li, 2008; Liggio et al., 2007; Liggio and Li, 2006). With regard to the role of $NH_3$ in SA formation, knowledge is still limited. In previous studies, inconsistent impacts of $NH_3$ on SA formation have been reported under different precursor systems. For example, $NH_3$ could elevate SA formation in the α-pinene/ozone oxidation system through acid-base reactions (Na et al., 2007), while the effects of $NH_3$ neutralization were masked by other multiple factors

and did not show significant influence on isoprene-derived SOA formation (Lin et al., 2013), and addition of $NH_3$ even significantly reduced the SA formation in the styrene/ozone system, which was caused by nucleophilic attack from the $NH_3$ molecule leading to rapid decomposition of the major aerosol products (Na et al., 2006). For the photo-oxidation of aromatic VOCs (e.g., toluene, o-/m-/p-xylene), the presence of $NH_3$ could facilitate new particle formation (NPF) and particle growth, subsequently leading to increased SA formation (Li et al., 2018; Liu et al., 2015b).

At the present time, the effects of $SO_2$ and $NH_3$ on SA formation have rarely been studied under highly complex pollution conditions (Chu et al., 2016). Vehicular evaporative emissions have been reported to be non-negligible contributors (39.20 %) to ambient VOCs from anthropogenic sources compared with vehicular tailpipe emissions (Liu et al., 2017a). In addition to short-chain alkanes, a certain proportion of aromatics and alkanes (C6 to C12) were also contained in the evaporative emissions (Liu et al., 2008; Zhang et al., 2013). Previous studies have reported that aromatics and long-chain (C6 to C19) alkanes, which are intermediate volatility organic compounds (IVOCs) (Donahue et al., 2006), could contribute to SOA formation (Pye and Pouliot, 2012; Tkacik et al., 2012; Lim and Ziemann, 2005). Therefore, it is necessary to study the influence of $SO_2$ and $NH_3$ on SA formation from evaporative emissions.

In this study, unburned gasoline vapors were used as a substitute for evaporative emissions, and the roles of $SO_2$ and $NH_3$ on SA formation from the photo-oxidation of unburned gasoline vapors were investigated in a 30 $m^3$ indoor smog chamber, in order to understand the formation potential of SA from oxidation of gasoline vapor in the cocktail of pollutants in Beijing. The respective influences of $SO_2$ and $NH_3$ on both the microphysics and chemistry of SA formation were examined. Meanwhile, the chemical compositions of the formed SOA in the presence of $SO_2$ and $NH_3$ were further explored by applying positive matrix factorization (PMF) analysis. The formation potentials of SA, sulfur- and nitrogen-containing

organics from vehicular evaporative emissions in the presence of $SO_2$ and $NH_3$ were evaluated and discussed.

# 2 Materials and Methods

## 2.1 Gasoline fuel

The utilized gasoline fuel with grade 92# was collected (refer to the standard Method for manual sampling of petroleum liquids (GB/T 4756-2015)) from a gas station located in Beijing. The gasoline complies with the China V gasoline fuel standard. It contains 65.1 % (v/v) alkanes (C6 to C12), 22.8 % (v/v) aromatics (mainly including benzene, toluene, xylene, trimethylbenzene) and 12.1 % (v/v) alkenes. The composition of the gasoline is similar to the gasoline collected in North China reported by Tang et al. (2015) and could represent the gasoline used in most areas of China for studying SA formation potential. Details of the gasoline composition are given in Table S1.

## 2.2 Smog chamber facility

A series of photochemical experiments with unburned gasoline vapors in the absence or presence of $SO_2$ or $NH_3$ were performed in a 30 $m^3$ indoor smog chamber at the Research Center for Eco-Environmental Sciences, Chinese Academy of Sciences (RCEES-CAS). The detailed schematic structure of the indoor smog chamber is given in Fig. S1 in the Supplement and described elsewhere (Chen et al., 2019a, b). Briefly, the cuboid chamber reactor (L × W × H = 3.0 × 2.5 × 4.0 m, S/V = 1.97 $m^{-1}$) was irradiated by 120 UV lamps (Philips) with peak intensity at 365 nm, providing a $NO_2$ photolysis rate of 0.55 $min^{-1}$. The interior was coated with 125 μm-thick FEP100 film (DuPont™, US) and the chamber was located in a temperature-controlled room, in which the temperature (T) and relative humidity (RH) could be controlled mechanically. A three-wing stainless-steel fan coated with Teflon was installed inside the reactor to guarantee that the gas and particle phase species mix sufficiently before photochemical reaction.

The chamber was also equipped with a series of gas- and particle-phase monitoring instruments. For

gaseous $NO_x$, $O_3$ and $SO_2$, a chemiluminescence analyzer (Model 42i-TL, Thermo Fisher Scientific, USA), a UV photometric analyzer (Model 49i, Thermo Fisher Scientific, USA) and a pulsed fluorescence analyzer (Model 43i, Thermo Fisher Scientific, USA) were used to monitor the concentrations in real time, respectively. The VOC species in gasoline were measured with a gas chromatograph (7890B GC, Agilent, USA) equipped with a DB-624 column (60 m × 0.25 mm × 1.40 μm, Agilent, USA) and a mass spectrometry detector (5977A MS, Agilent, USA) (GC-MS). In addition, proton-transfer-reaction time of flight mass spectrometry (PTR-TOF) (Ionicon Analytik GmbH, Austria) was also used for the measurement of gas-phase hydrocarbons and their intermediate products (Yuan et al., 2017). The size distribution and number concentration of the formed particulate matter (PM) were measured using a scanning mobility particle sizer (SMPS, TSI, USA), which was composed of a differential mobility analyzer (DMA, 3080 Classifier, TSI, USA) coupled with a condensation particle counter (CPC, 3776, TSI, USA). The mass concentration was estimated based on the volume concentration and the density of PM calculated from the equation $\rho = d_{va}/d_m$, where $d_{va}$ is the mean vacuum aerodynamic diameter measured by an Aerodyne high-resolution time-of-flight aerosol mass spectrometer (HR-ToF-AMS) and $d_m$ is the mean electrical mobility diameter measured by SMPS (DeCarlo et al., 2004). The calculated density of PM ranged from 1.5 to 1.6 g $cm^{-3}$ in the different reaction systems, which was in the range of density of SOA derived from aromatic hydrocarbons (1.24−1.48 g $cm^{-3}$) (Sato et al., 2010) and ammonium nitrate ($NH_4NO_3$, 1.72 g $cm^{-3}$) (Bahreini et al., 2005) and could be comparable with the previous studies (Li et al., 2018). The mass concentration and chemical composition of PM were simultaneously monitored using a high-resolution time-of-flight aerosol mass spectrometer (HR-ToF-AMS, Aerodyne Research Inc. USA). For all experiments, the HR-ToF-AMS operated in a cycle including two modes, 3 min V mode and 2 min W mode. Specifically, V mode (higher signal) can obtain the mass concentrations of the aerosols and W mode (higher resolution) can obtain high resolution mass spectral

data. The inlet flow rate, ionization efficiency (IE), and particle sizing were calibrated according to the standard protocols (Drewnick et al., 2005; Jimenez et al., 2003; Jayne et al., 2000), using the size-selected pure ammonium nitrate (AN) particles. All HR-ToF-AMS data were analyzed with ToF-AMS analysis toolkit SQUIRREL 1.57I/PIKA 1.16I version, in Igor Pro Version 6.37. HR-ToF-AMS results were also corrected using the mass concentration derived from SMPS according to the same method as Gordon et al. (2014), details of this correction are shown in the Supplement. As for the RH control system, it is achieved by vaporizing Milli-Q ultrapure water contained in a 5.0 L high pressure resistant container and the water vapor is flushed with purified dry zero air into the chamber. T and RH were monitored real-time using a hydro-thermometer (Vaisala HMP110) during the entirety of each experiment.

**2.3 Wall loss corrections**

The measured particle concentration was corrected in accordance with the relationship between the deposition rate ($k_{dep}$) and particle diameter ($D_p$, nm) (i.e., $k_{dep} = 4.15 \times 10^{-7} \times D_p^{1.89} + 1.39 \times D_p^{-0.88}$), which was described by Takekawa et al. (2003). The wall loss rates of $NO_2$, NO, $O_3$, $SO_2$ and VOC species were determined to be $(1.67 \pm 0.25) \times 10^{-4}$, $(1.32 \pm 0.32) \times 10^{-4}$, $(3.32 \pm 0.21) \times 10^{-4}$, $(4.52 \pm 0.11) \times 10^{-4}$ and $(2.20 \pm 0.39) \times 10^{-4}$ $min^{-1}$, respectively. Therefore, the wall loss of gas phase species was evaluated to be less than 5% of their maximum concentration in this study.

Wall losses of semi-volatile organic compounds (SVOCs) and low-volatility organic compounds (LVOCs) would lead to a substantial underestimation of SA formation (Krechmer et al., 2016; Ye et al., 2016; Zhang et al., 2015; Zhang et al., 2014), which is caused by the competition between these vapors condensing onto particles versus onto chamber walls. This competition could be evaluated by the corresponding timescales associated with reaching gas-to-particle partitioning equilibrium ($\bar{\tau}_{g\text{-}p}$) and vapor wall loss ($\tau_{g\text{-}w}$) (Zhang et al., 2014), and this underestimation of SA formation could be approximately quantified by the

ratio of these two timescales (i.e., $\bar{\tau}_{g\text{-}p}/\tau_{g\text{-}w}$). According to the methods described by Zhang et al. (2014), $\bar{\tau}_{g\text{-}p}$ and $\tau_{g\text{-}w}$ could be estimated assuming an upper bound and a lower bound of the molecular mass of organic vapors (MW) (100−300 g $mol^{-1}$) (as discussed in the Supplement). In order to accurately quantify the SA formation, the underestimation caused by the loss of SVOCs and LVOCs (include sulfuric acid gas) to the chamber walls was taken into account in this study. In this study, the SA yields were underestimated by a factor of 1.97−2.82 fold when considering the ratio of these two timescales (i.e., $\bar{\tau}_{g\text{-}p}/\tau_{g\text{-}w}$), which showed a decreasing trend with the increase of the $SO_2$ and $NH_3$ initial concentrations, suggesting that an increasing proportion of vapors is partitioned onto the suspended particle surface rather than the chamber wall.

**2.4 Experimental conditions**

Prior to each experiment, the chamber reactor was flushed by purified and dry zero air for about 24−36 h at a flow rate of 100 L $min^{-1}$ until almost no gas-phase species (i.e., $NO_x$, $O_3$ and $SO_2$) could be detected (< 1 ppb) and the particle number concentration was < 10 $cm^{-3}$. Before the experiments, the chamber was humidified to ~50 % RH by passing purified zero air through ultra-pure water (18.2 MΩ, Millipore Milli-Q). After that, a known volume of liquid gasoline (100 μL) was injected into the chamber through a heated Teflon line system (~100 °C) carried by purified dry zero air to ensure that all were evaporated into the chamber. Subsequently, NO, $SO_2$ or/and $NH_3$ were successively injected into the chamber from standard gas cylinders using mass flow controllers. The initial VOCs/$NO_x$ ratio (ppbC $ppb^{-1}$) was kept constant (Table 1). In order to reduce the adsorption of $NH_3$ in the pipeline, the $NH_3$ flow in a bypass line was balanced for about 30 min before it was injected into the chamber. The concentrations of NO and $SO_2$ were continuously monitored until they were stable, ensuring that the gaseous species mixed well in the chamber. For the concentration of $NH_3$, the value was estimated according to the amount of $NH_3$ introduced and the volume of the reactor chamber. The experiment was then conducted for about 8 h after turning off the fan and turning

on the UV lights. All the experiments were performed at a temperature of 26 ± 1 °C and wet conditions (RH = 50 ± 3 %). The detailed experimental conditions are listed in Table 1. The letters in the abbreviations represent the reactants introduced into the chamber reactor for each experiment. For example, SGN is an experiment with the presence of sulfur dioxide (S), gasoline vapor (G), and nitrogen oxides (N). Four experiments (Exps. SGN1, SGN2, SGN3, and SGN4) were carried out at different $SO_2$ initial concentrations. AGN is an experiment with the presence of ammonia (A), gasoline vapor (G), and nitrogen oxides (N). Two experiments (Exps. AGN1 and AGN2) were carried out at different $NH_3$ initial concentrations.

# 3 Results and discussion

## 3.1 Effect of $SO_2$ and $NH_3$ on the gas-phase species

Time-resolved concentrations of inorganic and organic gas-phase species during the photo-oxidation of gasoline/$NO_x$ in the absence or presence of $SO_2$ and $NH_3$ are shown in Fig. S2 and Fig. S3 in the Supplement, respectively. After turning on the UV lights, NO was rapidly converted to $NO_2$. At the same time, $O_3$ was gradually generated, with a maximum concentration of up to 350 ppb (Fig. S2). As shown in Fig. S2, there was no obvious difference in the variation of $NO_x$ and $O_3$ in the presence of $SO_2$ or $NH_3$. Additionally, the decay of typical VOC precursors (e.g., benzene, toluene, methylcyclopentane, methylcyclohexane) measured by PTR-TOF and GC-MS are given in Fig. S3, which traced very closely with each other (Fig. S4, in the Supplement). There were also no observable differences in these precursors VOCs among these experiments. According to the decay curves of aromatic hydrocarbons, the OH radical concentrations were estimated to be (7.54−8.40) × $10^6$ molecules $cm^{-3}$, which were also similar among these experiments. This was consistent with the previous study conducted by Chu et al. (2016), who found that the presence of $SO_2$ and $NH_3$ did not significantly impact the OH concentration during the photo-oxidation of toluene in the presence of $NO_x$.

However, as for the gas-phase intermediates formed during the photo-oxidation of gasoline/$NO_x$ under different conditions, such as small molecule oxygenated VOCs (OVOCs), which could also be measured by PTR-TOF. The time series of OVOCs concentration would vary with the concentration of $SO_2$ and $NH_3$. For example, we observed that acetic acid concentration decreased with the increased concentration of $SO_2$ (Fig. S5, in the Supplement), suggesting that the uptake of acetic acid may be enhanced. This phenomenon was consistent with those reported by Liggio and Li (2006), who observed that the uptake of organic compounds under acidic conditions would be enhanced significantly. Moreover, the presence of high concentrations of $SO_2$ would generate gaseous $H_2SO_4$, which would contribute to the formation of particle phase, as discussed in the next section. Similarly, the concentration of acetic acid also shown an obviously decreased trend in the presence of $NH_3$ (Fig. S5, in the Supplement), which could be caused by the reaction of acid-base reaction or the uptake of acetic acid in the presence of $NH_3$ (Liu et al., 2015c).

### 3.2 Role of $SO_2$ in secondary aerosol formation

To investigate the effects of $SO_2$ on SA formation from the photo-oxidation of gasoline/$NO_x$, smog chamber experiments with different $SO_2$ initial concentrations were carried out (Table 1). As shown in Fig. 1, compared to the experiments without the addition of $SO_2$, the SA concentration was enhanced to different degrees (1.6−2.6 times) in the presence of different $SO_2$ concentrations (35−151 ppb, i.e., 100−431 μg $m^{-3}$). As for each chemical species (i.e., organics, nitrate, sulfate, and ammonium), they all showed a trend of linear increase with the increase of $SO_2$ concentration (Fig. 2), especially for the sulfate ($k = 8.4\times10^{-2}$) and organic aerosol ($k = 2.9\times10^{-2}$). Previous studies have also revealed its promoting role on SA formation from different precursors (Zhao et al., 2018; Liu et al., 2017b; Díaz-de-Mera et al., 2017; Liu et al., 2016; Chu et al., 2016).

Additionally, the particle number concentrations and size growth were greatly enhanced by the presence

of $SO_2$. As evident from Fig. 3, the corresponding maximal particle number concentrations ($5.82 \times 10^4$–$1.91 \times 10^5$ $cm^{-3}$) were significantly enhanced by a factor of 2.9–3.3 in the presence of $SO_2$. This universal phenomenon has been reported by many studies (Díaz-de-Mera et al., 2017; Liu et al., 2017b; Liu et al., 2016; Chu et al., 2016). For example, the maximal particle number concentrations were enhanced by the presence of $SO_2$ (~130 ppb) to one order of magnitude in the photo-oxidation of high concentration toluene/$NO_x$ (Chu et al., 2016). For complex precursor systems (gasoline vehicle exhaust), Liu et al. (2016) have also found that under high $SO_2$ concentration (~150 ppb) conditions, the maximum particle number concentrations increased by 5.4–48 times compared to those without $SO_2$ during the photo-oxidation of gasoline vehicle exhaust. This higher magnification of $SO_2$ might be related to the different VOCs composition between evaporative emissions and gasoline vehicle exhaust, especially the aromatic and IVOCs (Liu et al., 2017). Our recent study demonstrated that SOA formation could be significantly enhanced by the increase of aromatic content (Chen et al., 2019b). Those unspeciated organic emissions (e.g., IVOCs) from gasoline vehicle exhaust would also have a significant contribution to SOA formation (Jathar et al., 2014; Gordon et al., 2014). Moreover, a small amount of POA was present in the initial reaction systems in Liu et al. (2016). These enhanced SOA formation and the pre-existing POA would provide larger surface areas for the condensation and heterogeneous uptake of low-volatility vapors (e.g., gaseous $H_2SO_4$), then promoting a higher magnification in particle number concentrations in the presence of $SO_2$. The higher initial mixing ratios of precursors (2.2–4.3 ppm) was also present in the reaction systems conducted by Liu et al. (2016), which would further be beneficial to the SOA formation. In addition, size distributions of generated SA in smaller size ranges (4–160 nm) were also determined using another SMPS equipped with a nanometer differential mobility analyzer (Nano-DMA), indicating that the new particle formation (NPF) phenomenon was enhanced significantly when the $SO_2$ concentration increased (Fig. S6). The presence of high

concentrations of $SO_2$ would generate sulfuric acid ($H_2SO_4$), which would contribute to nucleation and increase the total particle number concentrations (Zhao et al., 2018; Sipilä et al., 2010). As the $SO_2$ concentration increased from 35 ppb to 151 ppb, the maximal particle diameters (144−172 nm) became larger, which will have a direct impact on the scattering and absorption of light (Seinfeld and Pandis, 2016). An enhancement effect of $SO_2$ on the surface area of particles was also observed. As shown in Table 1, the surface area of aerosol particles at the end of each experiment increased from $1.12 \times 10^3$ to $2.46 \times 10^3$ $\mu m^2$ $cm^{-3}$ when the $SO_2$ concentration increased from 0 to 151 ppb. The larger surface area would be beneficial to the condensation and heterogeneous uptake of low-volatility vapors (Chapleski et al., 2016), consequently leading to higher SA yield in the presence of $SO_2$ (Table 1) (Santiago et al., 2012). Additionally, it is worth noting that there was a discrepancy between the magnification of particle number concentrations, surface areas and $SO_2$ concentrations. On one hand, there might be some particles, especially nanoclusters, were lost to the chamber wall and not be detected; on the other hand, the initial size of nanoclusters contributed from gaseous $H_2SO_4$ was small enough (sub-3 nm) (Chu et al., 2019; Sipilä et al., 2010) and couldn't be detected by our general SMPS. That is to say, the particle number concentrations and surface areas measured by our SMPS might be the particles after growing up by collision. This could be supported by the enhancement in the particle diameters (144−172 nm) and sulfate concentrations (13−38 $\mu g\ m^{-3}$) in the presence of $SO_2$. After considering the underestimation of particles formation (factor of 1.97−2.82, seen in Section 2.3), the sulfate concentrations will be enhanced by a factor of 5.8 when comparing between experiments SGN 1 and SGN 4.

In order to further investigate the role of $SO_2$ in the chemistry of SOA formation, the particle acidities were estimated using the E-AIM model (Model II: $H^+$ - $NH_4^+$ - $SO_4^{2-}$ - $NO_3^-$ - $H_2O$) (Clegg and Brimblecombe, 2005; Wexler and Clegg, 2002; Clegg et al., 1998). The concentrations of chemical components (i.e., $NH_4^+$,

280 $SO_4^{2-}$, and $NO_3^-$) at the time when the SOA formation rate reached its peak were used as the inputs of the
281 model. As shown in Fig. 4, the $H^+$ concentration was increased from 8.5 to 32.5 nmol $m^{-3}$ with the increase
282 of $SO_2$ concentration under moderate humidity conditions (RH = 50 %) and the higher SOA concentration
283 and SOA yield could be well explained by the enhancement of the particle acidities ($R^2$ = 0.960 and $R^2$ =
284 0.986, respectively). The higher SOA concentration and SOA yield were related to the acid-catalyzed
285 reactions of multifunctional aldehydes (e.g., glyoxal and methylglyoxal), which were the products of
286 aromatic hydrocarbons in the gasoline vapors through the gas-phase photo-oxidation. Hemiacetals, acetals
287 and alcohols could be generated through the acid-catalyzed heterogeneous reactions of glyoxal (Czoschke
288 et al., 2003; Jang et al., 2002). These low-vapor-pressure products generated from heterogeneous reactions
289 preferentially contribute to the SOA formation (Kroll and Seinfeld, 2008; Cao and Jang, 2007; Casale et al.,
290 2007; Jang et al., 2002).

291 In addition, the sulfur-containing organics formed in the presence of $SO_2$ might be another reason for
292 the increase of SOA yield (Kundu et al., 2013; Liggio et al., 2005). Jaoui et al. (2008) have reported that the
293 acidic aerosol generated in the presence of $SO_2$ could lead to sulfur-incorporating reactions in the particle
294 phase during the photo-oxidation of α-pinene/toluene/$NO_x$ mixtures. Sulfur-containing organics could be
295 generated via reactions of organic species (e.g., polycyclic aromatic hydrocarbons (PAHs), C10−C12 alkanes,
296 alcohols, epoxides) with sulfate, bisulfate or sulfuric acid, especially under high relative humidity and acidity
297 conditions (Riva et al., 2015, 2016; Huang et al., 2015; Hatch et al., 2011; Surratt et al., 2007; Liggio et al.,
298 2005). Huang et al. (2015) have revealed that sulfur-containing organics with R-O-$SO_3^-$ functional groups
299 will yield S-bearing organic fragments ($C_xH_yO_zS$) during ionization, which subsequently could be detected
300 by HR-ToF-AMS and used as marker ions to quantify them. In our gasoline/$NO_x$ experiments in the presence
301 of $SO_2$, the ions $CSO^+$, $CH_3SO_2^+$ and $CH_3SO_3^+$ could be separated (Fig. S7), although uncertainty might be

induced in the peak-fitting of the highly abundant ions $C_2H_4O_2^+$, $C_6H_7^+$, and $C_5H_3O_2^+$. These characteristic ions (i.e., $CSO^+$, $CH_3SO_2^+$ and $CH_3SO_3^+$) also have been observed from sulfur-containing organics in previous field measurements (Huang et al., 2015; Farmer et al., 2010). According to the estimation method for sulfur-containing organics mentioned in Huang et al. (2015), we found that the signal of these ions and the concentrations of sulfur-containing organics increased with the $SO_2$ initial concentration (Fig. 5). The conservative lower-bound estimated concentrations of sulfur-containing organics (13−26 ng $m^{-3}$) were comparable to those (~ 20 ng $m^{-3}$) observed in the mid-Atlantic United States, which were derived from biogenic and anthropogenic hydrocarbons (Meade et al., 2016). Additionally, it should be noted that the sulfur-containing organics concentration in this study might be underestimated by the HR-ToF-AMS when considering one cannot resolve all the sulfur-containing fragments that may exist, and some of the sulfur-containing organics might fragment into masses that do not contain sulfur and thus are quantified as organic. Furthermore, the relative ionization efficiency (RIE) for the sulfur-containing organics fragments was assumed to be equivalent to the remainder of the organics (1.3), since a RIE value for sulfur-containing organics is unknown. This may introduce an additional uncertainty to the quantitation of sulfur-containing organics. Therefore, photo-oxidation of gasoline vapor in the presence of $SO_2$ might be a noteworthy source of sulfur-containing organics, although the concentration was very low compared to that of generated $SO_4^{2-}$ (~ 0.1% of $SO_4^{2-}$).

### 3.3 Role of $NH_3$ in secondary aerosol formation

Similarly, the role of $NH_3$ in SA formation was examined. It is worth noting that ammonium aerosols were formed without the addition of gaseous $NH_3$ (Fig. S8, in the Supplement), which signified that some $NH_3$ was present in the background air in the chamber or introduced during the humidification process of the chamber (Liu et al., 2015c). Unfortunately, appropriate instruments are unavailable to measure the exact

concentration of background $NH_3$ in the chamber. According to the concentration of generated ammonium aerosols, the concentration of background $NH_3$ was estimated to be ~15 ppb using the E-AIM model (Clegg and Brimblecombe, 2005; Wexler and Clegg, 2002; Clegg et al., 1998). Therefore, for the experiments with the presence of $NH_3$, the concentration of injected $NH_3$ (150−200 ppb) was much higher than this value to identify the effect of $NH_3$ on SA formation. The SA concentration was enhanced by a factor of 2.0−2.5 in the presence of $NH_3$, as shown in Fig. S9a. The formation of SOA, $NO_3^-$ and $NH_4^+$ was enhanced to varying degrees. The increase of $NO_3^-$ and $NH_4^+$ could be attributed to the formation of inorganic $NH_4NO_3$ in the presence of $NH_3$. The $NO^+/NO_2^+$ ratio, which could be derived from HR-ToF-AMS, has often been used as a proxy for identification of inorganic nitrate and organic nitrogen compounds (Farmer et al., 2010; Sato et al., 2010; Rollins et al., 2009). Generally, the $NO^+/NO_2^+$ ratio of inorganic nitrate (1.08−2.81) is lower than that of organic nitrogen compounds (3.82−5.84) (Liu et al., 2016). In this study, the $NO^+/NO_2^+$ ratio became substantially lower (~ 2.00) in the presence of $NH_3$ compared with that in the absence of $NH_3$ (~ 5.46). Therefore, $NH_4NO_3$ was the dominant nitrate species in the presence of $NH_3$. As for the reason for SOA enhancement, the presence of $NH_3$ could react with some organic acids and subsequently contribute to SOA formation (Na et al., 2007; Na et al., 2006), which could be supported by the increase of N/C (from 0.016 to 0.033) with increasing $NH_3$ concentration at similar concentrations of $NO_x$. In addition, we have found that the presence of $NH_3$ readily increased the particle diameter and number concentration of SA generated in the photo-oxidation of gasoline (Figs. S9b and S9c), which revealed that $NH_3$ played an important role in new particle formation (NPF). These are consistent with the simulation results finding that $NH_3$ promotes atmospheric NPF and also the conversion of $SO_2$ and $NO_2$ (Jiang and Xia, 2017). The increased surface area of particles was also observed (Table 1, $2.07 \times 10^3$ and $2.48 \times 10^3$ $\mu m^2$ $cm^{-3}$) as the $NH_3$ concentration increased from 0 to 150 and 200 ppb. Similarly, the larger surface area would favor the partitioning of low-

346 volatility vapors to the particle phase, leading to the higher SA yield (Table 1).

347 Previous studies have reported that the reaction of carbonyl compounds (e.g., glyoxal) could be
348 catalyzed by $NH_4^+$ ions through a Bronsted acid pathway or an iminium pathway, which could generate N-
349 containing products and oligomers (Nozière et al., 2009), and then contribute a substantial fraction to SOA
350 (Liu et al., 2015c; Farmer et al., 2010; Cheng et al., 2006). Researchers have identified the characteristic
351 fragments of nitrogen-containing organics as $C_xH_yN_n$ and $C_xH_yO_zN_n$ using HR-ToF-AMS (Lee et al., 2013;
352 Farmer et al., 2010; Galloway et al., 2009). In this study, the typical normalized mass spectrum of N-
353 containing fragments in SOA after 480 min of photo-oxidation reaction at different concentrations of $NH_3$
354 are given in Fig. 6. The prominent peaks in the $C_xH_yN_n$ family were at *m/z* 27 ($CHN^+$), 30 ($CH_4N^+$),
355 40($C_2H_2N^+$), 41($CHN_2^+$, $C_2H_3N^+$), 42($C_2H_4N^+$), 43($C_2H_5N^+$), 54($C_2H_2N_2^+$, $C_3H_4N^+$), 55($C_3H_5N^+$), and
356 68($C_3H_4N_2^+$, $C_4H_6N^+$); and the $C_xH_yO_zN_n$ fragments were dominated by 45($CH_3ON^+$), 46($CH_4ON^+$),
357 59($C_2H_5ON^+$), 63($CH_5O_2N^+$), 73($C_2H_5ON_2^+$, $C_3H_7ON^+$), 86($C_3H_4O_2N^+$, $C_3H_6ON_2^+$), 91($C_3H_9O_2N^+$),
358 97($C_4H_5ON_2^+$), and 104($C_3H_6O_3N^+$, $C_4H_{10}O_2N^+$). The N-containing fragments observed in the experiment
359 without added $NH_3$ could be attributed to the reactions between organic peroxy ($RO_2$) radicals and $NO_x$
360 (Arey et al., 2001) or uptake of background $NH_3$ by SOA. Additionally, it was obvious that the signal
361 intensities of most N-containing fragments became significantly stronger as the $NH_3$ concentration increased
362 (150−200 ppb). Therefore, a considerable amount of nitrogen-containing organics (the ratio of nitrogen-
363 containing organics to SOA was about 6.7−7.7%) was formed during the photo-oxidation of gasoline vapor
364 in the presence of $NH_3$. This was consistent with the previous study conducted by Liu et al. (2015c), who
365 observed the formation of organic nitrogen compounds in the SOA generated from the OH oxidation of m-
366 xylene. The promoting role of $NH_3$ in the formation of N-containing species was also observed in the reaction
367 system of ozonolysis and photo-oxidation of α-pinene (Babar et al., 2017).

In addition, elemental analysis was also carried out to elucidate the SOA chemical composition and SOA formation mechanisms (Chhabra et al., 2011; Heald et al., 2010) at different concentrations of $NH_3$. The time evolution of H/C and O/C in SOA formed from the photo-oxidation of gasoline vapor at different concentrations of $NH_3$ is shown in Fig. 7. As evident from Fig. 7, all data points are located in the triangular area for slope between -1 and 0, which suggests that SOA formation from the photo-oxidation of gasoline vapor is a combination of carboxylic acid and alcohol/peroxide (Heald et al., 2010). Moreover, in the presence of $NH_3$, as shown in Fig. 8, N/C increased as reaction proceeded in the initial oxidation stage (0−120 min), accompanied by a rapid increase of O/C (0.12−0.67), a decrease of H/C (2.12−1.61), and a rapid formation of SOA. During this stage, the photo-oxidation of VOC precursors leads to a rapid increase in O/C and a rapid decrease in H/C. The termination chemistry of $NO_x$ with free radicals and the $NH_3$ uptake result in a rapid increase in N/C. As the reaction proceeded further (120−300 min), an increase of H/C which should be caused by $NH_3$ uptake resulted in an almost constant oxidation state of SOA in the continuous photo-oxidation, accompanied by an increase in the SOA concentration. Nozière et al. (2009) have reported that N-containing products would be generated from carbonyl compound (e.g., glyoxal) self-reactions catalyzed by $NH_4^+$ ions, which will have a dramatic impact on the volatility of oxidation products and the yield of SOA (Ortiz-Montalvo et al., 2014). In the last stage of the reaction (360−480 min), $NH_3$ uptake might reach saturation; therefore, H/C and N/C are almost constant. Comparing experiments with different concentrations of $NH_3$, the average H/C shows an obvious increase (1.53−1.70) while the average O/C (0.70−0.78) shows a slight increase with the increase of $NH_3$ concentration (0−200 ppb), seen in Fig. S10. The slope in the Van Krevelen diagram shows a trend from slope = -1 to slope = 0 (Fig. S10), indicating that the formed carboxylic acid would further react with $NH_3$ via acid-base reaction to generate an ammonium salt of a carboxylate anion in the presence of $NH_3$ (Na et al., 2007). Xu et al. (2018) recently found that

imidazole products containing multiple oxygen atoms could be generated through heterogeneous reactions between $NH_3$ and carbonyl compounds (e.g., glyoxal), which might also contribute to the increase in the O/C of the SOA.

### 3.4 Different roles of $SO_2$ and $NH_3$ in SOA chemical properties

The chemical properties of the SOA generated under the different concentration of $SO_2$ or $NH_3$ were further compared by applying positive matrix factorization (PMF) analysis to the HR-ToF-AMS data, respectively (Chu et al., 2016; Liu et al., 2014). The details of PMF analysis are given in the Supplement. For the experiments under different $SO_2$ concentration conditions (i.e., Exps. GN, SGN1, SGN2, SGN3 and SGN4), two factors (Factor 1-S and Factor 2-S, Fig. S11a) were identified from the PMF analysis, and the difference mass spectra (*m/z* 12−170) between the two factors and the time series of the mass concentrations are shown in Fig. 9. The intensity of $C_xH_y$ and S-bearing organic fragments ($C_xH_yO_zS$) in Factor 1-S was obviously stronger than that in Factor 2-S. Meanwhile, fragments in the high *m/z* range (> 110 Da) were more abundant in Factor 1-S (Fig. 9a, marked in red box). By contrast, the fragments containing oxygen in Factor 2-S were more abundant than in Factor 1-S, such as the typical fragment $CO_2^+$ (*m/z* 44). Therefore, Factor 1-S was tentatively assigned to the less-oxygenated organic aerosol and oligomers, while Factor 2-S was more-oxygenated organic aerosol (Ulbrich et al., 2009). Similarly, for the experiments at different $NH_3$ concentration (i.e., Exps. GN, AGN1 and AGN2), two factors (Factor 1-N and Factor 2-N, Fig. S11b) were also identified in the same way. According to Fig. 10, Factor 1-N was tentatively assigned to the less-oxygenated organic aerosol and oligomers, while Factor 2-N was more-oxygenated organic aerosol and nitrogen-containing organics.

As shown in Fig. 9b and Fig. 10b, these two factors both had different time series during the entire reaction. With respect to Exps. GN, SGN1, SGN2, SGN3 and SGN4, Factor 1-S was formed later (~ 30 min)

than Factor 2-S, and then continuously increased during the entire reaction. Comparing experiments with different $SO_2$ concentrations, the maximum concentration of Factor 1-S, which was related to the less-oxygenated organic aerosol and oligomers, was enhanced with increased $SO_2$ concentration ($R^2$ = 0.881, Fig. 9c). This suggested that the presence of $SO_2$ was prone to decrease the oxidation state of organic aerosol via acid-catalyzed reactions and enhance the formation of oligomers (Liu et al., 2016), which was consistent with the evolution of O/C vs. H/C shown in Fig. S12. Moreover, the gradually increasing concentration of Factor 1-S was related to the formation of sulfur-containing organics in the presence of $SO_2$ (Blair et al., 2017). By contrast, Factor 2-S was first gradually increased with the progress of the reaction and then decreased after reaching a peak (i.e., inflection point). And the time to reach the inflection point was affected by the $SO_2$ concentration (Fig. 9b). As the initial concentration of $SO_2$ increased from 0 ppb to 151 ppb, the time corresponding to the inflection point decreased, which indicated that the adverse influence of acid catalysis on Factor 2-S was gradually enhanced. In addition, the maximum concentration of Factor 2-S was negatively related with $SO_2$ concentration ($R^2$ = 0.987, Fig. 9c); this suggested that the presence of $SO_2$ and acid catalysis was adverse to the formation of more-oxygenated organic aerosol, leading to the decrease of the oxidation state of organic aerosol (Fig. S12).

By contrast, for Exps. GN, AGN1 and AGN2, Factor 1-N was first increased with the progress of the reaction and then gradually decreased after reaching a peak (Fig. 10b); while Factor 2-N was formed later (~ 30 min) than Factor 1-N, and then continuously increased during the entire reaction. This phenomenon was consistent with the expected behavior, that less-oxidized organic aerosol would be further oxidized to form more-oxidized organic aerosol. When comparing experiments with different $NH_3$ concentrations, it was observed that the concentration of Factor 2-N increased with increasing $NH_3$ concentration. Meanwhile, Factor 2-N, which was related to the more-oxidized organic aerosol and nitrogen-containing organics, was

a dominant factor in the presence of $NH_3$, and its maximum concentration was enhanced with the increase in $NH_3$ concentration ($R^2$ = 0.988, Fig. 10c). Thence, the formation of more-oxygenated organic aerosol and nitrogen-containing organics will be enhanced with the increase of $NH_3$ concentration. In contrast, a negative correlation was observed between the maximum concentration of Factor 1-N and $NH_3$ concentration ($R^2$ = 0.876, Fig. 10c); this revealed that less-oxygenated organic aerosol was gradually transformed to more oxidized species and nitrogen-containing organics in the presence of $NH_3$.

# 4 Conclusions

In this study, SA formation from the photo-oxidation of gasoline/$NO_x$ in the presence of $SO_2$ or $NH_3$ was investigated. Our experimental results demonstrated that SA was enhanced by a factor of 1.6−2.6 or 2.0−2.5, respectively, with the increase of $SO_2$ or $NH_3$ concentration (0−151 ppb and 0−200 ppb, respectively). Meanwhile, both secondary organic aerosol (SOA) and secondary inorganic aerosol (SIA) were increased by varying degrees. In the presence of $SO_2$, $SO_4^{2-}$ was the most sensitive linear increase with the increase of $SO_2$ concentration, and SOA was also greatly enhanced due to the acid catalytic effect and the formation of sulfur-containing organics. In the presence of $NH_3$, $NH_4NO_3$ was most enhanced, following by SOA. The formation of nitrogen-containing organics was also promoted by the presence of $NH_3$. Meanwhile, conspicuous new particle formation (NPF) and particle size growth were enhanced in the presence of $SO_2$ or $NH_3$.

In this study, a linear relationship between the SA yield and $SO_2$ or $NH_3$ concentration was also obtained (Fig. S13). Considering the typical concentrations of $SO_2$ and $NH_3$ of 40 ppb and 23 ppb in haze pollution in the north China plain (Cheng et al., 2016), and the lower aromatics content (~ 10%) in vehicular evaporative emissions (Zhang et al., 2013), the SA yield is roughly estimated to be about 0.20. Recently, an updated emission inventory of vehicular evaporative emissions was reported to be 1.65 Tg $yr^{-1}$ (Liu et al.,

2017a). Then, the SA formed from the photo-oxidation of VOCs emitted by vehicular evaporation in the presence of $SO_2$ and $NH_3$ is roughly estimated to be 0.33 Tg $yr^{-1}$, which is about 1.5 times as much as the primary $PM_{2.5}$ emissions from transportation (0.21 Tg $yr^{-1}$) in China (Jing et al., 2015; Zhang et al., 2007) and accounting for about 21 % of the SOA production (1.6 Tg $yr^{-1}$) from anthropogenic precursors estimated by global chemical transport model (Farina et al., 2010). In addition, the photo-oxidation of long-chain alkanes (> C6, IVOCs) contained in evaporative emissions would also contribute to SOA formation (Pye and Pouliot, 2012; Tkacik et al., 2012; Presto et al., 2009; Lim and Ziemann, 2005; Zhao et al., 2016). This estimate suggests that vehicular evaporative emissions will be a significant source of SA in the presence of $SO_2$ and $NH_3$, although the estimate might have a high uncertainty due to the fact that SA yield might vary considerably under different atmospheric conditions. Meanwhile, in the presence of $NO_x$, $SO_2$ and $NH_3$, vehicular evaporative emissions may be a potential source of sulfur- and nitrogen-containing organics, according to the results obtained from our study. Sulfur- and nitrogen-containing organics will have an adverse influence on the climate by light absorption and/or by affecting aerosol hygroscopicity (Staudt et al., 2014; Nguyen et al., 2012), and they also have a significant contribution to SOA and nitrogen or sulfur budgets (Lee et al., 2016; Shang et al., 2016).

Therefore, under the compound pollution conditions of $SO_2$ and $NH_3$, synergistic emission reduction of vehicular evaporative emissions, $SO_2$ (e.g., coal-fired flue gas) and $NH_3$ (e.g., emitted from agricultural non-point source and traffic emissions) should be taken into consideration by policy makers for future management, which will contribute to reducing the burden of $PM_{2.5}$, and then cut the environmental, economic and health costs caused by PM pollution. Our work will provide a scientific basis for taking corresponding control measures to relieve haze events in China. Additionally, there might be some differences between the VOCs composition of gasoline vapors directly injected to the smog chamber and

vehicular evaporative emissions. Thus, further work should be focused on SA formation directly from vehicular evaporative emissions under coexisting $SO_2$ and $NH_3$ conditions to shed light on the formation mechanism of SA under more atmospherically relevant conditions.

## Author contributions

TZC and YCL contributed equally to this work and should be considered as co-first authors. HH, QXM, YCL, and TZC proposed the initial idea. YCL and TZC designed and led the study. YCL, BWC, QXM, PZ, and TZC conducted the data analyses. TZC, YCL, BWC, PZ, CGL, and JL interpreted the data. TZC, YCL, JL, and QXM wrote the manuscript, with inputs from all coauthors.

## Acknowledgements

This work was financially supported by the National Key R&D Program of China (2016YFC0202700, 2018YFC0506901), the National Natural Science Foundation of China (21876185, 41877306, 41877304, and 91744205), the special fund of the State Key Joint Laboratory of Environment Simulation and Pollution Control (17L01ESPC), the Youth Innovation Promotion Association, CAS (2018055, 2018060, and 2017064), the Key Research Program of Frontier Sciences, CAS (QYZDB-SSW-DQC018), the National research program for key issues in air pollution control (DQGG0103), and the Young Talent Project of the Center for Excellence in Regional Atmospheric Environment, CAS (CERAE201801).

## References

Arey, J., Aschmann, S. M., Kwok, E. S. C., and Atkinson, R.: Alkyl nitrate, hydroxyalkyl nitrate, and hydroxycarbonyl formation from the $NO_x$−air photooxidations of $C_5$−$C_8$ n-alkanes, J. Phys. Chem. A, 105, 1020-1027, doi: 10.1021/jp003292z, 2001.

Atkinson, R., and Arey, J.: Atmospheric degradation of volatile organic compounds, Chem. Rev., 103, 4605-4638, doi: 10.1021/cr0206420, 2003.

Babar, Z. B., Park, J.-H., and Lim, H.-J.: Influence of $NH_3$ on secondary organic aerosols from the ozonolysis and photooxidation of α-pinene in a flow reactor, Atmos. Environ., 164, 71-84, doi: 10.1016/j.atmosenv.2017.05.034, 2017.

Bahreini, R., Keywood, M. D., Ng, N. L., Varutbangkul, V., Gao, S., Flagan, R. C., Seinfeld, J. H., Worsnop, D. R., and Jimenez, J. L.: Measurements of secondary organic aerosol from oxidation of cycloalkenes, terpenes, and m-xylene using an Aerodyne aerosol mass spectrometer, Environ. Sci. Technol., 39, 5674-5688, doi: 10.1021/es048061a, 2005.

Bauduin, S., Clarisse, L., Hadji-Lazaro, J., Theys, N., Clerbaux, C., and Coheur, P. F.: Retrieval of near-surface sulfur dioxide ($SO_2$) concentrations at a global scale using IASI satellite observations, Atmo. Meas. Tech., 9, 721-740, doi: 10.5194/amt-9-721-2016, 2016.

Blair, S. L., MacMillan, A. C., Drozd, G. T., Goldstein, A. H., Chu, R. K., Paša-Tolić, L., Shaw, J. B., Tolić, N., Lin, P., Laskin, J., Laskin, A., and Nizkorodov, S. A.: Molecular characterization of organosulfur compounds in biodiesel and diesel fuel secondary organic aerosol, Environ. Sci. Technol., 51, 119-127, doi: 10.1021/acs.est.6b03304, 2017.

Calvert, J. G., Atkinson, R., Becker, K. H., Kamens, R. M., Seinfeld, J. H., Wallington, T. H., and Yarwood, G.: The mechanisms of atmospheric oxidation of the aromatic hydrocarbons, Oxford University Press, 2002.

Cao, G., and Jang, M.: Effects of particle acidity and UV light on secondary organic aerosol formation from oxidation of aromatics in the absence of $NO_x$, Atmos. Environ., 41, 7603-7613, doi: 10.1016/j.atmosenv.2007.05.034, 2007.

Casale, M. T., Richman, A. R., Elrod, M. J., Garland, R. M., Beaver, M. R., and Tolbert, M. A.: Kinetics of acid-catalyzed aldol condensation reactions of aliphatic aldehydes, Atmos. Environ., 41, 6212-6224, doi: 10.1016/j.atmosenv.2007.04.002, 2007.

Chapleski, R. C., Zhang, Y., Troya, D., and Morris, J. R.: Heterogeneous chemistry and reaction dynamics of the atmospheric oxidants, $O_3$, $NO_3$, and OH, on organic surfaces, Chem. Soc. Rev., 45, 3731-3746, doi: 10.1039/C5CS00375J, 2016.

Chen, T., Liu, Y., Chu, B., Liu, C., Liu, J., Ge, Y., Ma, Q., Ma, J., and He, H.: Differences of the oxidation process and secondary organic aerosol formation at low and high precursor concentrations, J. Environ. Sci., 79, 256-263, doi: 10.1016/j.jes.2018.11.011, 2019a.

Chen, T., Liu, Y., Liu, C., Liu, J., Chu, B., and He, H.: Important role of aromatic hydrocarbons in SOA formation from unburned gasoline vapor, Atmos. Environ., 201, 101-109, doi: 10.1016/j.atmosenv.2019.01.001, 2019b.

Cheng, Y., Li, S.-M., and Leithead, A.: Chemical characteristics and origins of nitrogen-containing organic compounds in $PM_{2.5}$ aerosols in the Lower Fraser Valley, Environ. Sci. Technol., 40, 5846-5852, doi: 10.1021/es0603857, 2006.

Cheng, Y., Zheng, G., Wei, C., Mu, Q., Zheng, B., Wang, Z., Gao, M., Zhang, Q., He, K., Carmichael, G., Pöschl, U., and Su, H.: Reactive nitrogen chemistry in aerosol water as a source of sulfate during haze events in China, Sci. Adv., 2, doi: 10.1126/sciadv.1601530, 2016.

Chhabra, P. S., Ng, N. L., Canagaratna, M. R., Corrigan, A. L., Russell, L. M., Worsnop, D. R., Flagan, R. C., and Seinfeld, J. H.: Elemental composition and oxidation of chamber organic aerosol, Atmos. Chem. Phys., 11, 8827-8845, doi: 10.5194/acp-11-8827-2011, 2011.

Chu, B., Kerminen, V. M., Bianchi, F., Yan, C., Petäjä, T., and Kulmala, M.: Atmospheric new particle formation in China, Atmos. Chem. Phys., 19, 115-138, doi: 10.5194/acp-19-115-2019, 2019.

Chu, B., Zhang, X., Liu, Y., He, H., Sun, Y., Jiang, J., Li, J., and Hao, J.: Synergetic formation of secondary inorganic and organic aerosol: effect of $SO_2$ and $NH_3$ on particle formation and growth, Atmos. Chem. Phys., 16,

14219-14230, doi: 10.5194/acp-16-14219-2016, 2016.

Clegg, S. L., Brimblecombe, P., and Wexler, A. S.: Thermodynamic model of the system $H^+$–$NH_4^+$–$SO_4^{2-}$–$NO_3^-$–$H_2O$ at tropospheric temperatures, J. Phys. Chem. A, 102, 2137-2154, doi: 10.1021/jp973042r, 1998.

Clegg, S. L., and Brimblecombe, P.: Comment on the "Thermodynamic Dissociation Constant of the Bisulfate Ion from Raman and Ion Interaction Modeling Studies of Aqueous Sulfuric Acid at Low Temperatures", J. Phys. Chem. A, 109, 2703-2706, doi: 10.1021/jp0401170, 2005.

Czoschke, N. M., Jang, M., and Kamens, R. M.: Effect of acidic seed on biogenic secondary organic aerosol growth, Atmos. Environ., 37, 4287-4299, doi: 10.1016/S1352-2310(03)00511-9, 2003.

Davidson, C. I., Phalen, R. F., and Solomon, P. A.: Airborne particulate matter and human health: a review, Aerosol Sci. Tech., 39, 737-749, doi: 10.1080/02786820500191348, 2005.

DeCarlo, P. F., Slowik, J. G., Worsnop, D. R., Davidovits, P., and Jimenez, J. L.: Particle morphology and density characterization by combined mobility and aerodynamic diameter measurements. Part 1: Theory, Aerosol Sci. Tech., 38, 1185-1205, doi: 10.1080/027868290903907, 2004.

Díaz-de-Mera, Y., Aranda, A., Martínez, E., Rodríguez, A. A., Rodríguez, D., and Rodríguez, A.: Formation of secondary aerosols from the ozonolysis of styrene: effect of $SO_2$ and $H_2O$, Atmos. Environ., 171, 25-31, doi: 10.1016/j.atmosenv.2017.10.011, 2017.

Donahue, N. M., Robinson, A. L., Stanier, C. O., and Pandis, S. N.: Coupled partitioning, dilution, and chemical aging of semivolatile organics, Environ. Sci. Technol., 40, 2635-2643, doi: 10.1021/es052297c, 2006.

Drewnick, F., Hings, S. S., DeCarlo, P., Jayne, J. T., Gonin, M., Fuhrer, K., Weimer, S., Jimenez, J. L., Demerjian, K. L., Borrmann, S., and Worsnop, D. R.: A new time-of-flight aerosol mass spectrometer (TOF-AMS)—instrument description and first field deployment, Aerosol Sci. Tech., 39, 637-658, doi: 10.1080/02786820500182040, 2005.

Edney, E. O., Kleindienst, T. E., Jaoui, M., Lewandowski, M., Offenberg, J. H., Wang, W., and Claeys, M.: Formation of 2-methyl tetrols and 2-methylglyceric acid in secondary organic aerosol from laboratory irradiated isoprene/$NO_x$/$SO_2$/air mixtures and their detection in ambient $PM_{2.5}$ samples collected in the eastern United States, Atmos. Environ., 39, 5281-5289, doi: 10.1016/j.atmosenv.2005.05.031, 2005.

Farmer, D. K., Matsunaga, A., Docherty, K. S., Surratt, J. D., Seinfeld, J. H., Ziemann, P. J., and Jimenez, J. L.: Response of an aerosol mass spectrometer to organonitrates and organosulfates and implications for atmospheric chemistry, Proc. Natl. Acad. Sci. USA, 107, 6670-6675, doi: 10.1073/pnas.0912340107, 2010.

Fu, X., Wang, S. X., Ran, L. M., Pleim, J. E., Cooter, E., Bash, J. O., Benson, V., and Hao, J. M.: Estimating $NH_3$ emissions from agricultural fertilizer application in China using the bi-directional CMAQ model coupled to an agro-ecosystem model, Atmos. Chem. Phys., 15, 6637-6649, doi: 10.5194/acp-15-6637-2015, 2015.

Galloway, M. M., Chhabra, P. S., Chan, A. W. H., Surratt, J. D., Flagan, R. C., Seinfeld, J. H., and Keutsch, F. N.: Glyoxal uptake on ammonium sulphate seed aerosol: reaction products and reversibility of uptake under dark and irradiated conditions, Atmos. Chem. Phys., 9, 3331-3345, doi: 10.5194/acp-9-3331-2009, 2009.

Gordon, T. D., Presto, A. A., May, A. A., Nguyen, N. T., Lipsky, E. M., Donahue, N. M., Gutierrez, A., Zhang, M., Maddox, C., Rieger, P., Chattopadhyay, S., Maldonado, H., Maricq, M. M., and Robinson, A. L.: Secondary organic aerosol formation exceeds primary particulate matter emissions for light-duty gasoline vehicles, Atmos. Chem. Phys., 14, 4661-4678, doi: 10.5194/acp-14-4661-2014, 2014.

Guo, S., Hu, M., Zamora, M. L., Peng, J., Shang, D., Zheng, J., Du, Z., Wu, Z., Shao, M., Zeng, L., Molina, M. J., and Zhang, R.: Elucidating severe urban haze formation in China, Proc. Natl. Acad. Sci. USA, 111, 17373-17378, doi: 10.1073/pnas.1419604111, 2014.

Hallquist, M., Wenger, J. C., Baltensperger, U., Rudich, Y., Simpson, D., Claeys, M., Dommen, J., Donahue, N. M., George, C., Goldstein, A. H., Hamilton, J. F., Herrmann, H., Hoffmann, T., Iinuma, Y., Jang, M., Jenkin,

M. E., Jimenez, J. L., Kiendler-Scharr, A., Maenhaut, W., McFiggans, G., Mentel, T. F., Monod, A., Prévôt, A. S. H., Seinfeld, J. H., Surratt, J. D., Szmigielski, R., and Wildt, J.: The formation, properties and impact of secondary organic aerosol: current and emerging issues, Atmos. Chem. Phys., 9, 5155-5236, doi: 10.5194/acp-9-5155-2009, 2009.

Hatch, L. E., Creamean, J. M., Ault, A. P., Surratt, J. D., Chan, M. N., Seinfeld, J. H., Edgerton, E. S., Su, Y., and Prather, K. A.: Measurements of isoprene-derived organosulfates in ambient aerosols by aerosol time-of-flight mass spectrometry—Part 2: temporal variability and formation mechanisms, Environ. Sci. Technol., 45, 8648-8655, doi: 10.1021/es2011836, 2011.

He, H., Wang, Y., Ma, Q., Ma, J., Chu, B., Ji, D., Tang, G., Liu, C., Zhang, H., and Hao, J.: Mineral dust and $NO_x$ promote the conversion of $SO_2$ to sulfate in heavy pollution days, Sci. Rep., 4, 4172, doi: 10.1038/srep04172, 2014.

Heald, C. L., Kroll, J. H., Jimenez, J. L., Docherty, K. S., DeCarlo, P. F., Aiken, A. C., Chen, Q., Martin, S. T., Farmer, D. K., and Artaxo, P.: A simplified description of the evolution of organic aerosol composition in the atmosphere, Geophys. Res. Lett., 37, L08803, doi: 10.1029/2010GL042737, 2010.

Hou, S., Tong, S., Ge, M., and An, J.: Comparison of atmospheric nitrous acid during severe haze and clean periods in Beijing, China, Atmos. Environ., 124, 199-206, doi: 10.1016/j.atmosenv.2015.06.023, 2016.

Huang, D. D., Li, Y. J., Lee, B. P., and Chan, C. K.: Analysis of organic sulfur compounds in atmospheric aerosols at the HKUST supersite in Hong Kong using HR-ToF-AMS, Environ. Sci. Technol., 49, 3672-3679, doi: 10.1021/es5056269, 2015.

Huang, R.-J., Zhang, Y., Bozzetti, C., Ho, K.-F., Cao, J.-J., Han, Y., Daellenbach, K. R., Slowik, J. G., Platt, S. M., Canonaco, F., Zotter, P., Wolf, R., Pieber, S. M., Bruns, E. A., Crippa, M., Ciarelli, G., Piazzalunga, A., Schwikowski, M., Abbaszade, G., Schnelle-Kreis, J., Zimmermann, R., An, Z., Szidat, S., Baltensperger, U.,

610 Haddad, I. E., and Prevot, A. S. H.: High secondary aerosol contribution to particulate pollution during haze events
611 in China, Nature, 514, 218-222, doi: 10.1038/nature13774, 2014.
612 Ianniello, A., Spataro, F., Esposito, G., Allegrini, I., Rantica, E., Ancora, M. P., Hu, M., and Zhu, T.:
613 Occurrence of gas phase ammonia in the area of Beijing (China), Atmos. Chem. Phys., 10, 9487-9503, doi:
614 10.5194/acp-10-9487-2010, 2010.
615 Jang, M., and Kamens, R. M.: Atmospheric secondary aerosol formation by heterogeneous reactions of
616 aldehydes in the presence of a sulfuric acid aerosol catalyst, Environ. Sci. Technol., 35, 4758-4766, doi:
617 10.1021/es010790s, 2001.
618 Jang, M., Czoschke, N. M., Lee, S., and Kamens, R. M.: Heterogeneous atmospheric aerosol production by
619 acid-catalyzed particle-phase reactions, Science, 298, 814-817, doi: 10.1126/science.1075798, 2002.
620 Jang, M., Carroll, B., Chandramouli, B., and Kamens, R. M.: Particle growth by acid-catalyzed
621 heterogeneous reactions of organic carbonyls on preexisting aerosols, Environ. Sci. Technol., 37, 3828-3837, doi:
622 10.1021/es021005u, 2003a.
623 Jang, M., Lee, S., and Kamens, R. M.: Organic aerosol growth by acid-catalyzed heterogeneous reactions of
624 octanal in a flow reactor, Atmos. Environ., 37, 2125-2138, doi: 10.1016/S1352-2310(03)00077-3, 2003b.
625 Jaoui, M., Edney, E. O., Kleindienst, T. E., Lewandowski, M., Offenberg, J. H., Surratt, J. D., and Seinfeld,
626 J. H.: Formation of secondary organic aerosol from irradiated α-pinene/toluene/$NO_x$ mixtures and the effect of
627 isoprene and sulfur dioxide, J. Geophys. Res.-Atmos., 113, doi: 10.1029/2007jd009426, 2008.
628 Jathar, S. H., Gordon, T. D., Hennigan, C. J., Pye, H. O. T., Pouliot, G., Adams, P. J., Donahue, N. M., and
629 Robinson, A. L.: Unspeciated organic emissions from combustion sources and their influence on the secondary
630 organic aerosol budget in the United States, Proc. Natl. Acad. Sci. USA, 111, 10473-10478, doi:
631 10.1073/pnas.1323740111, 2014.

Jayne, J. T., Leard, D. C., Zhang, X., Davidovits, P., Smith, K. A., Kolb, C. E., and Worsnop, D. R.: Development of an aerosol mass spectrometer for size and composition analysis of submicron particles, Aerosol Sci. Tech., 33, 49-70, doi: 10.1080/027868200410840, 2000.

Jiang, B., and Xia, D.: Role identification of $NH_3$ in atmospheric secondary new particle formation in haze occurrence of China, Atmos. Environ., 163, 107-117, doi: 10.1016/j.atmosenv.2017.05.035, 2017.

Jimenez, J. L., Canagaratna, M. R., Donahue, N. M., Prevot, A. S. H., Zhang, Q., Kroll, J. H., DeCarlo, P. F., Allan, J. D., Coe, H., Ng, N. L., Aiken, A. C., Docherty, K. S., Ulbrich, I. M., Grieshop, A. P., Robinson, A. L., Duplissy, J., Smith, J. D., Wilson, K. R., Lanz, V. A., Hueglin, C., Sun, Y. L., Tian, J., Laaksonen, A., Raatikainen, T., Rautiainen, J., Vaattovaara, P., Ehn, M., Kulmala, M., Tomlinson, J. M., Collins, D. R., Cubison, M. J., Dunlea, J., Huffman, J. A., Onasch, T. B., Alfarra, M. R., Williams, P. I., Bower, K., Kondo, Y., Schneider, J., Drewnick, F., Borrmann, S., Weimer, S., Demerjian, K., Salcedo, D., Cottrell, L., Griffin, R., Takami, A., Miyoshi, T., Hatakeyama, S., Shimono, A., Sun, J. Y., Zhang, Y. M., Dzepina, K., Kimmel, J. R., Sueper, D., Jayne, J. T., Herndon, S. C., Trimborn, A. M., Williams, L. R., Wood, E. C., Middlebrook, A. M., Kolb, C. E., Baltensperger, U., and Worsnop, D. R.: Evolution of organic aerosols in the atmosphere, Science, 326, 1525-1529, doi: 10.1126/science.1180353, 2009.

Jimenez, J. L., Jayne, J. T., Shi, Q., Kolb, C. E., Worsnop, D. R., Yourshaw, I., Seinfeld, J. H., Flagan, R. C., Zhang, X., Smith, K. A., Morris, J. W., and Davidovits, P.: Ambient aerosol sampling using the aerodyne aerosol mass spectrometer, J Geophys Res Atmos, 108, doi: 10.1029/2001JD001213, 2003.

Jing, M., Junfeng, L., Yuan, X., and Shu, T.: Tracing primary $PM_{2.5}$ emissions via Chinese supply chains, Environ. Res. Lett., 10, 054005, 2015.

Kang, Y., Liu, M., Song, Y., Huang, X., Yao, H., Cai, X., Zhang, H., Kang, L., Liu, X., Yan, X., He, H., Zhang, Q., Shao, M., and Zhu, T.: High-resolution ammonia emissions inventories in China from 1980 to 2012,

654 Atmos. Chem. Phys., 16, 2043-2058, doi: 10.5194/acp-16-2043-2016, 2016.

655 Kleindienst, T. E., Edney, E. O., Lewandowski, M., Offenberg, J. H., and Jaoui, M.: Secondary organic
656 carbon and aerosol yields from the irradiations of isoprene and α-pinene in the presence of $NO_x$ and $SO_2$, Environ.
657 Sci. Technol., 40, 3807-3812, doi: 10.1021/es052446r, 2006.

658 Krechmer, J. E., Pagonis, D., Ziemann, P. J., and Jimenez, J. L.: Quantification of gas-wall partitioning in
659 Teflon environmental chambers using rapid bursts of low-volatility oxidized species generated in situ, Environ.
660 Sci. Technol., 50, 5757-5765, doi: 10.1021/acs.est.6b00606, 2016.

661 Kroll, J. H., Donahue, N. M., Jimenez, J. L., Kessler, S. H., Canagaratna, M. R., Wilson, K. R., Altieri, K.
662 E., Mazzoleni, L. R., Wozniak, A. S., Bluhm, H., Mysak, E. R., Smith, J. D., Kolb, C. E., and Worsnop, D. R.:
663 Carbon oxidation state as a metric for describing the chemistry of atmospheric organic aerosol, Nat. Chem., 3,
664 133, doi: 10.1038/nchem.948, 2011.

665 Kroll, J. H., and Seinfeld, J. H.: Chemistry of secondary organic aerosol: Formation and evolution of low-
666 volatility organics in the atmosphere, Atmos. Environ., 42, 3593-3624, doi: 10.1016/j.atmosenv.2008.01.003,
667 2008.

668 Kundu, S., Quraishi, T. A., Yu, G., Suarez, C., Keutsch, F. N., and Stone, E. A.: Evidence and quantitation
669 of aromatic organosulfates in ambient aerosols in Lahore, Pakistan, Atmos. Chem. Phys., 13, 4865-4875, doi:
670 10.5194/acp-13-4865-2013, 2013.

671 Lee, A. K. Y., Zhao, R., Li, R., Liggio, J., Li, S.-M., and Abbatt, J. P. D.: Formation of light absorbing organo-
672 nitrogen species from evaporation of droplets containing glyoxal and ammonium sulfate, Environ. Sci. Technol.,
673 47, 12819-12826, doi: 10.1021/es402687w, 2013.

674 Lee, B. H., Mohr, C., Lopez-Hilfiker, F. D., Lutz, A., Hallquist, M., Lee, L., Romer, P., Cohen, R. C., Iyer,
675 S., Kurtén, T., Hu, W., Day, D. A., Campuzano-Jost, P., Jimenez, J. L., Xu, L., Ng, N. L., Guo, H., Weber, R. J.,

Wild, R. J., Brown, S. S., Koss, A., de Gouw, J., Olson, K., Goldstein, A. H., Seco, R., Kim, S., McAvey, K., Shepson, P. B., Starn, T., Baumann, K., Edgerton, E. S., Liu, J., Shilling, J. E., Miller, D. O., Brune, W., Schobesberger, S., D'Ambro, E. L., and Thornton, J. A.: Highly functionalized organic nitrates in the southeast United States: Contribution to secondary organic aerosol and reactive nitrogen budgets, Proc. Natl. Acad. Sci. USA, 113, 1516-1521, doi: 10.1073/pnas.1508108113, 2016.

Li, K., Chen, L., White, S. J., Yu, H., Wu, X., Gao, X., Azzi, M., and Cen, K.: Smog chamber study of the role of $NH_3$ in new particle formation from photo-oxidation of aromatic hydrocarbons, Sci. Total Environ., 619-620, 927-937, doi: 10.1016/j.scitotenv.2017.11.180, 2018.

Li, L., Tan, Q., Zhang, Y., Feng, M., Qu, Y., An, J., and Liu, X.: Characteristics and source apportionment of $PM_{2.5}$ during persistent extreme haze events in Chengdu, southwest China, Environ. Pollut., 230, 718-729, doi: 10.1016/j.envpol.2017.07.029, 2017.

Liggio, J., Li, S.-M., and McLaren, R.: Heterogeneous reactions of glyoxal on particulate matter: identification of acetals and sulfate esters, Environ. Sci. Technol., 39, 1532-1541, doi: 10.1021/es048375y, 2005.

Liggio, J., and Li, S. M.: Reactive uptake of pinonaldehyde on acidic aerosols, J. Geophys. Res.-Atmos., 111, doi: doi:10.1029/2005JD006978, 2006.

Liggio, J., Li, S. M., Brook, J. R., and Mihele, C.: Direct polymerization of isoprene and α-pinene on acidic aerosols, Geophys. Res. Lett., 34, doi: 10.1029/2006GL028468, 2007.

Liggio, J., and Li, S. M.: Reversible and irreversible processing of biogenic olefins on acidic aerosols, Atmos. Chem. Phys., 8, 2039-2055, doi: 10.5194/acp-8-2039-2008, 2008.

Lim, Y. B., and Ziemann, P. J.: Products and mechanism of secondary organic aerosol formation from reactions of n-alkanes with OH radicals in the presence of $NO_x$, Environ. Sci. Technol., 39, 9229-9236, doi: 10.1021/es051447g, 2005.

Lin, Y. H., Knipping, E. M., Edgerton, E. S., Shaw, S. L., and Surratt, J. D.: Investigating the influences of $SO_2$ and $NH_3$ levels on isoprene-derived secondary organic aerosol formation using conditional sampling approaches, Atmos. Chem. Phys., 13, 8457-8470, doi: 10.5194/acp-13-8457-2013, 2013.

Liu, H., Man, H., Cui, H., Wang, Y., Deng, F., Wang, Y., Yang, X., Xiao, Q., Zhang, Q., Ding, Y., and He, K.: An updated emission inventory of vehicular VOCs and IVOCs in China, Atmos. Chem. Phys., 17, 12709-12724, doi: 10.5194/acp-17-12709-2017, 2017a.

Liu, S., Jia, L., Xu, Y., Tsona, N. T., Ge, S., and Du, L.: Photooxidation of cyclohexene in the presence of $SO_2$: SOA yield and chemical composition, Atmos. Chem. Phys., 17, 13329-13343, doi: 10.5194/acp-17-13329-2017, 2017b.

Liu, T., Wang, X., Deng, W., Hu, Q., Ding, X., Zhang, Y., He, Q., Zhang, Z., Lü, S., Bi, X., Chen, J., and Yu, J.: Secondary organic aerosol formation from photochemical aging of light-duty gasoline vehicle exhausts in a smog chamber, Atmos. Chem. Phys., 15, 9049-9062, doi: 10.5194/acp-15-9049-2015, 2015a.

Liu, T., Wang, X., Deng, W., Zhang, Y., Chu, B., Ding, X., Hu, Q., He, H., and Hao, J.: Role of ammonia in forming secondary aerosols from gasoline vehicle exhaust, Sci. China Chem., 58, 1377-1384, doi: 10.1007/s11426-015-5414-x, 2015b.

Liu, T., Wang, X., Hu, Q., Deng, W., Zhang, Y., Ding, X., Fu, X., Bernard, F., Zhang, Z., Lü, S., He, Q., Bi, X., Chen, J., Sun, Y., Yu, J., Peng, P., Sheng, G., and Fu, J.: Formation of secondary aerosols from gasoline vehicle exhaust when mixing with $SO_2$, Atmos. Chem. Phys., 16, 675-689, doi: 10.5194/acp-16-675-2016, 2016.

Liu, X. G., Li, J., Qu, Y., Han, T., Hou, L., Gu, J., Chen, C., Yang, Y., Liu, X., Yang, T., Zhang, Y., Tian, H., and Hu, M.: Formation and evolution mechanism of regional haze: a case study in the megacity Beijing, China, Atmos. Chem. Phys., 13, 4501-4514, doi: 10.5194/acp-13-4501-2013, 2013.

Liu, Y., Li, S. M., and Liggio, J.: Technical Note: application of positive matrix factor analysis in

heterogeneous kinetics studies utilizing the mixed-phase relative rates technique, Atmos. Chem. Phys., 14, 9201-9211, doi: 10.5194/acp-14-9201-2014, 2014.

Liu, Y., Liggio, J., Staebler, R., and Li, S. M.: Reactive uptake of ammonia to secondary organic aerosols: kinetics of organonitrogen formation, Atmos. Chem. Phys., 15, 13569-13584, doi: 10.5194/acp-15-13569-2015, 2015c.

Liu, Y., Shao, M., Fu, L., Lu, S., Zeng, L., and Tang, D.: Source profiles of volatile organic compounds (VOCs) measured in China: Part I, Atmos. Environ., 42, 6247-6260, doi: 10.1016/j.atmosenv.2008.01.070, 2008.

Lu, Z., Streets, D. G., Zhang, Q., Wang, S., Carmichael, G. R., Cheng, Y. F., Wei, C., Chin, M., Diehl, T., and Tan, Q.: Sulfur dioxide emissions in China and sulfur trends in East Asia since 2000, Atmos. Chem. Phys., 10, 6311-6331, doi: 10.5194/acp-10-6311-2010, 2010.

Meade, L. E., Riva, M., Blomberg, M. Z., Brock, A. K., Qualters, E. M., Siejack, R. A., Ramakrishnan, K., Surratt, J. D., and Kautzman, K. E.: Seasonal variations of fine particulate organosulfates derived from biogenic and anthropogenic hydrocarbons in the mid-Atlantic United States, Atmos. Environ., 145, 405-414, doi: 10.1016/j.atmosenv.2016.09.028, 2016.

Meng, Z. Y., Lin, W. L., Jiang, X. M., Yan, P., Wang, Y., Zhang, Y. M., Jia, X. F., and Yu, X. L.: Characteristics of atmospheric ammonia over Beijing, China, Atmos. Chem. Phys., 11, 6139-6151, doi: 10.5194/acp-11-6139-2011, 2011.

Na, K., Song, C., and Cocker, D. R.: Formation of secondary organic aerosol from the reaction of styrene with ozone in the presence and absence of ammonia and water, Atmos. Environ., 40, 1889-1900, doi: 10.1016/j.atmosenv.2005.10.063, 2006.

Na, K., Song, C., Switzer, C., and Cocker, D. R.: Effect of ammonia on secondary organic aerosol formation from α-pinene ozonolysis in dry and humid conditions, Environ. Sci. Technol., 41, 6096-6102, doi:

742 10.1021/es061956y, 2007.

743 Nguyen, T. B., Lee, P. B., Updyke, K. M., Bones, D. L., Laskin, J., Laskin, A., and Nizkorodov, S. A.:
744 Formation of nitrogen- and sulfur-containing light-absorbing compounds accelerated by evaporation of water
745 from secondary organic aerosols, J. Geophys. Res.-Atmos., 117, doi: 10.1029/2011jd016944, 2012.

746 Nozière, B., Dziedzic, P., and Córdova, A.: Products and kinetics of the liquid-phase reaction of glyoxal
747 catalyzed by ammonium ions ($NH_4^+$), J. Phys. Chem. A, 113, 231-237, doi: 10.1021/jp8078293, 2009.

748 Ortiz-Montalvo, D. L., Häkkinen, S. A. K., Schwier, A. N., Lim, Y. B., McNeill, V. F., and Turpin, B. J.:
749 Ammonium addition (and aerosol pH) has a dramatic impact on the volatility and yield of glyoxal secondary
750 organic aerosol, Environ. Sci. Technol., 48, 255-262, doi: 10.1021/es4035667, 2014.

751 Pan, Y., Tian, S., Liu, D., Fang, Y., Zhu, X., Zhang, Q., Zheng, B., Michalski, G., and Wang, Y.: Fossil fuel
752 combustion-related emissions dominate atmospheric ammonia sources during severe haze episodes: Evidence
753 from 15N-stable isotope in size-resolved aerosol ammonium, Environ. Sci. Technol., 50, 8049-8056, doi:
754 10.1021/acs.est.6b00634, 2016.

755 Platt, S. M., El Haddad, I., Zardini, A. A., Clairotte, M., Astorga, C., Wolf, R., Slowik, J. G., Temime-Roussel,
756 B., Marchand, N., Ježek, I., Drinovec, L., Močnik, G., Möhler, O., Richter, R., Barmet, P., Bianchi, F.,
757 Baltensperger, U., and Prévôt, A. S. H.: Secondary organic aerosol formation from gasoline vehicle emissions in
758 a new mobile environmental reaction chamber, Atmos. Chem. Phys., 13, 9141-9158, doi: 10.5194/acp-13-9141-
759 2013, 2013.

760 Pöschl, U.: Atmospheric aerosols: composition, transformation, climate and health effects, Angew. Chem.
761 Int. Ed., 44, 7520-7540, doi: 10.1002/anie.200501122, 2005.

762 Presto, A. A., Miracolo, M. A., Kroll, J. H., Worsnop, D. R., Robinson, A. L., and Donahue, N. M.:
763 Intermediate-volatility organic compounds: A potential source of ambient oxidized organic aerosol, Environ. Sci.

764 Technol., 43, 4744-4749, doi: 10.1021/es803219q, 2009.

765 Pye, H. O. T., and Pouliot, G. A.: Modeling the role of alkanes, polycyclic aromatic hydrocarbons, and their
766 oligomers in secondary organic aerosol formation, Environ. Sci. Technol., 46, 6041-6047, doi:
767 10.1021/es300409w, 2012.

768 Riva, M., Tomaz, S., Cui, T., Lin, Y.-H., Perraudin, E., Gold, A., Stone, E. A., Villenave, E., and Surratt, J.
769 D.: Evidence for an unrecognized secondary anthropogenic source of organosulfates and sulfonates: gas-phase
770 oxidation of polycyclic aromatic hydrocarbons in the presence of sulfate aerosol, Environ. Sci. Technol., 49, 6654-
771 6664, doi: 10.1021/acs.est.5b00836, 2015.

772 Riva, M., Da Silva Barbosa, T., Lin, Y. H., Stone, E. A., Gold, A., and Surratt, J. D.: Chemical
773 characterization of organosulfates in secondary organic aerosol derived from the photooxidation of alkanes,
774 Atmos. Chem. Phys., 16, 11001-11018, doi: 10.5194/acp-16-11001-2016, 2016.

775 Rollins, A. W., Kiendler-Scharr, A., Fry, J. L., Brauers, T., Brown, S. S., Dorn, H. P., Dube, W. P., Fuchs, H.,
776 Mensah, A., Mentel, T. F., Rohrer, F., Tillmann, R., Wegener, R., Wooldridge, P. J., and Cohen, R. C.: Isoprene
777 oxidation by nitrate radical: Alkyl nitrate and secondary organic aerosol yields, Atmos. Chem. Phys., 9, 6685-
778 6703, doi: 10.5194/acp-9-6685-2009, 2009.

779 Santiago, M., Garcia Vivanco, M., and Stein, A. F.: $SO_2$ effect on secondary organic aerosol from a mixture
780 of anthropogenic VOCs: experimental and modelled results, Int. J. Environ. Pollut., 50, 224-233, doi:
781 10.1504/ijep.2012.051195, 2012.

782 Sato, K., Takami, A., Isozaki, T., Hikida, T., Shimono, A., and Imamura, T.: Mass spectrometric study of
783 secondary organic aerosol formed from the photo-oxidation of aromatic hydrocarbons, Atmos. Environ., 44, 1080-
784 1087, doi: 10.1016/j.atmosenv.2009.12.013, 2010.

785 Seinfeld, J. H., and Pandis, S. N.: Atmospheric chemistry and physics: from air pollution to climate change,

John Wiley & Sons, Hoboken, NJ, 2016.

Shang, J., Passananti, M., Dupart, Y., Ciuraru, R., Tinel, L., Rossignol, S., Perrier, S., Zhu, T., and George, C.: $SO_2$ uptake on oleic acid: a new formation pathway of organosulfur compounds in the atmosphere, Environ. Sci. Technol. Let., 3, 67-72, doi: 10.1021/acs.estlett.6b00006, 2016.

Shen, X. J., Sun, J. Y., Zhang, X. Y., Zhang, Y. M., Zhang, L., Che, H. C., Ma, Q. L., Yu, X. M., Yue, Y., and Zhang, Y. W.: Characterization of submicron aerosols and effect on visibility during a severe haze-fog episode in Yangtze River Delta, China, Atmos. Environ., 120, 307-316, doi: 10.1016/j.atmosenv.2015.09.011, 2015.

Sipilä, M., Berndt, T., Petäjä, T., Brus, D., Vanhanen, J., Stratmann, F., Patokoski, J., Mauldin, R. L., Hyvärinen, A.-P., Lihavainen, H., and Kulmala, M.: The role of sulfuric acid in atmospheric nucleation, Science, 327, 1243-1246, doi: 10.1126/science.1180315, 2010.

Staudt, S., Kundu, S., Lehmler, H.-J., He, X., Cui, T., Lin, Y.-H., Kristensen, K., Glasius, M., Zhang, X., Weber, R. J., Surratt, J. D., and Stone, E. A.: Aromatic organosulfates in atmospheric aerosols: synthesis, characterization, and abundance, Atmos. Environ., 94, 366-373, doi: 10.1016/j.atmosenv.2014.05.049, 2014.

Sun, K., Tao, L., Miller, D. J., Pan, D., Golston, L. M., Zondlo, M. A., Griffin, R. J., Wallace, H. W., Leong, Y. J., Yang, M. M., Zhang, Y., Mauzerall, D. L., and Zhu, T.: Vehicle emissions as an important urban ammonia source in the United States and China, Environ. Sci. Technol., 51, 2472-2481, doi: 10.1021/acs.est.6b02805, 2017.

Sun, Y., Chen, C., Zhang, Y., Xu, W., Zhou, L., Cheng, X., Zheng, H., Ji, D., Li, J., Tang, X., Fu, P., and Wang, Z.: Rapid formation and evolution of an extreme haze episode in Northern China during winter 2015, Sci. Rep., 6, 27151, doi: 10.1038/srep27151, 2016.

Surratt, J. D., Kroll, J. H., Kleindienst, T. E., Edney, E. O., Claeys, M., Sorooshian, A., Ng, N. L., Offenberg, J. H., Lewandowski, M., Jaoui, M., Flagan, R. C., and Seinfeld, J. H.: Evidence for organosulfates in secondary organic aerosol, Environ. Sci. Technol., 41, 517-527, doi: 10.1021/es062081q, 2007.

Takekawa, H., Minoura, H., and Yamazaki, S.: Temperature dependence of secondary organic aerosol formation by photo-oxidation of hydrocarbons, Atmos. Environ., 37, 3413-3424, doi: 10.1016/S1352-2310(03)00359-5, 2003.

Tan, J.-H., Duan, J.-C., Chen, D.-H., Wang, X.-H., Guo, S.-J., Bi, X.-H., Sheng, G.-Y., He, K.-B., and Fu, J.-M.: Chemical characteristics of haze during summer and winter in Guangzhou, Atmos. Res., 94, 238-245, doi: 10.1016/j.atmosres.2009.05.016, 2009.

Tang, G., Sun, J., Wu, F., Sun, Y., Zhu, X., Geng, Y., and Wang, Y.: Organic composition of gasoline and its potential effects on air pollution in North China, Sci. China Chem., 58, 1416-1425, doi: 10.1007/s11426-015-5464-0, 2015.

Thalman, R., de Sá, S. S., Palm, B. B., Barbosa, H. M. J., Pöhlker, M. L., Alexander, M. L., Brito, J., Carbone, S., Castillo, P., Day, D. A., Kuang, C., Manzi, A., Ng, N. L., Sedlacek Iii, A. J., Souza, R., Springston, S., Watson, T., Pöhlker, C., Pöschl, U., Andreae, M. O., Artaxo, P., Jimenez, J. L., Martin, S. T., and Wang, J.: CCN activity and organic hygroscopicity of aerosols downwind of an urban region in central Amazonia: seasonal and diel variations and impact of anthropogenic emissions, Atmos. Chem. Phys., 17, 11779-11801, doi: 10.5194/acp-17-11779-2017, 2017.

Tkacik, D. S., Presto, A. A., Donahue, N. M., and Robinson, A. L.: Secondary organic aerosol formation from intermediate-volatility organic compounds: cyclic, linear, and branched alkanes, Environ. Sci. Technol., 46, 8773-8781, doi: 10.1021/es301112c, 2012.

Tong, S., Hou, S., Zhang, Y., Chu, B., Liu, Y., He, H., Zhao, P., and Ge, M.: Exploring the nitrous acid (HONO) formation mechanism in winter Beijing: direct emissions and heterogeneous production in urban and suburban areas, Faraday Discuss., 189, 213-230, doi: 10.1039/c5fd00163c, 2016.

Ulbrich, I. M., Canagaratna, M. R., Zhang, Q., Worsnop, D. R., and Jimenez, J. L.: Interpretation of organic

components from positive matrix factorization of aerosol mass spectrometric data, Atmos. Chem. Phys., 9, 2891-2918, doi: 10.5194/acp-9-2891-2009, 2009.

Wexler, A. S., and Clegg, S. L.: Atmospheric aerosol models for systems including the ions $H^+$, $NH_4^+$, $Na^+$, $SO_4^{2-}$, $NO_3^-$, $Cl^-$, $Br^-$, and $H_2O$, J. Geophys. Res.-Atmos., 107, doi: 10.1029/2001jd000451, 2002.

Xu, J., Huang, M.-Q., Cai, S.-Y., Liao, Y.-M., Hu, C.-J., Zhao, W.-X., Gu, X.-J., and Zhang, W.-J.: Chemical composition and reaction mechanisms for aged p-xylene secondary organic aerosol in the presence of ammonia, J. Chin. Chem. Soc-taip, 65, 578-590, doi: 10.1002/jccs.201700249, 2018.

Yang, S., Yuesi, W., and Changchun, Z.: Measurement of the vertical profile of atmospheric $SO_2$ during the heating period in Beijing on days of high air pollution, Atmos. Environ., 43, 468-472, doi: 10.1016/j.atmosenv.2008.09.057, 2009.

Yang, W., Li, J., Wang, M., Sun, Y., and Wang, Z.: A case study of investigating secondary organic aerosol formation pathways in Beijing using an observation-based SOA Box Model, Aerosol Air Qual. Res., 18, 1606-1616, doi: 10.4209/aaqr.2017.10.0415, 2018.

Ye, P., Ding, X., Hakala, J., Hofbauer, V., Robinson, E. S., and Donahue, N. M.: Vapor wall loss of semi-volatile organic compounds in a Teflon chamber, Aerosol Sci. Tech., 50, 822-834, doi: 10.1080/02786826.2016.1195905, 2016.

Yuan, B., Koss, A. R., Warneke, C., Coggon, M., Sekimoto, K., and de Gouw, J. A.: Proton-transfer-reaction mass spectrometry: Applications in atmospheric sciences, Chem. Rev., 117, 13187-13229, doi: 10.1021/acs.chemrev.7b00325, 2017.

Zhang, L., Chen, Y., Zhao, Y., Henze, D. K., Zhu, L., Song, Y., Paulot, F., Liu, X., Pan, Y., Lin, Y., and Huang, B.: Agricultural ammonia emissions in China: reconciling bottom-up and top-down estimates, Atmos. Chem. Phys., 18, 339-355, doi: 10.5194/acp-18-339-2018, 2018.

852 Zhang, Q., Streets, D. G., He, K., and Klimont, Z.: Major components of China's anthropogenic primary
853 particulate emissions, Environ. Res. Lett., 2, doi: 10.1088/1748-9326/2/4/045027, 2007.
854 Zhang, X., Cappa, C. D., Jathar, S. H., McVay, R. C., Ensberg, J. J., Kleeman, M. J., and Seinfeld, J. H.:
855 Influence of vapor wall loss in laboratory chambers on yields of secondary organic aerosol, Proc. Natl. Acad. Sci.
856 USA, 111, 5802-5807, doi: 10.1073/pnas.1404727111, 2014.
857 Zhang, X., Schwantes, R. H., McVay, R. C., Lignell, H., Coggon, M. M., Flagan, R. C., and Seinfeld, J. H.:
858 Vapor wall deposition in Teflon chambers, Atmos. Chem. Phys., 15, 4197-4214, doi: 10.5194/acp-15-4197-2015,
859 2015.
860 Zhang, Y., Wang, X., Zhang, Z., Lü, S., Shao, M., Lee, F. S. C., and Yu, J.: Species profiles and normalized
861 reactivity of volatile organic compounds from gasoline evaporation in China, Atmos. Environ., 79, 110-118, doi:
862 10.1016/j.atmosenv.2013.06.029, 2013.
863 Zhao, B., Wang, S., Donahue, N. M., Jathar, S. H., Huang, X., Wu, W., Hao, J., and Robinson, A. L.:
864 Quantifying the effect of organic aerosol aging and intermediate-volatility emissions on regional-scale aerosol
865 pollution in China, Sci. Rep., 6, doi: 10.1038/srep28815, 2016.
866 Zhao, D., Schmitt, S. H., Wang, M., Acir, I. H., Tillmann, R., Tan, Z., Novelli, A., Fuchs, H., Pullinen, I.,
867 Wegener, R., Rohrer, F., Wildt, J., Kiendler-Scharr, A., Wahner, A., and Mentel, T. F.: Effects of $NO_x$ and $SO_2$ on
868 the secondary organic aerosol formation from photooxidation of α-pinene and limonene, Atmos. Chem. Phys., 18,
869 1611-1628, doi: 10.5194/acp-18-1611-2018, 2018.
870 Zhao, D., Song, X., Zhu, T., Zhang, Z., Liu, Y., and Shang, J.: Multiphase oxidation of $SO_2$ by $NO_2$ on $CaCO_3$
871 particles, Atmos. Chem. Phys., 18, 2481-2493, doi: 10.5194/acp-18-2481-2018, 2018.
872 Zheng, B., Zhang, Q., Zhang, Y., He, K. B., Wang, K., Zheng, G. J., Duan, F. K., Ma, Y. L., and Kimoto, T.:
873 Heterogeneous chemistry: a mechanism missing in current models to explain secondary inorganic aerosol

formation during the January 2013 haze episode in North China, Atmos. Chem. Phys., 15, 2031-2049, doi: 10.5194/acp-15-2031-2015, 2015.

Zou, Y., Deng, X. J., Zhu, D., Gong, D. C., Wang, H., Li, F., Tan, H. B., Deng, T., Mai, B. R., Liu, X. T., and Wang, B. G.: Characteristics of 1 year of observational data of VOCs, $NO_x$ and $O_3$ at a suburban site in Guangzhou, China, Atmos. Chem. Phys., 15, 6625-6636, doi: 10.5194/acp-15-6625-2015, 2015.

879 Table 1. Summary of experimental conditions in this study.

| Exp. [a] | RH (%) | T (°C) | $SO_2$ (ppb) | $NH_3$ [b] (ppb) | $HC_0$ (ppb) | $NO_{x,0}$ (ppb) | $HC_0/NO_{x,0}$ (ppbC $ppb^{-1}$) | Surface [c] ($\mu m^2\ cm^{-3}$) | ΔHC ($\mu g\ m^{-3}$) | Δ*M* ($\mu g\ m^{-3}$) | SA yield [d] |
|---|---|---|---|---|---|---|---|---|---|---|---|
| GN | 50±3 | 26±1 | − | − | 411.0 | 128.4 | 20.61 | $1.12\times10^3$ | 747.8 | 34.6 | 0.130 |
| SGN1 | 50±3 | 26±1 | 35 | − | 419.8 | 121.0 | 22.34 | $1.73\times10^3$ | 871.6 | 58.0 | 0.155 |
| SGN2 | 50±3 | 26±1 | 74 | − | 412.0 | 121.3 | 21.88 | $2.06\times10^3$ | 866.2 | 77.8 | 0.193 |
| SGN3 | 50±3 | 26±1 | 116 | − | 383.6 | 119.8 | 20.62 | $2.23\times10^3$ | 791.1 | 87.1 | 0.226 |
| SGN4 | 50±3 | 26±1 | 151 | − | 394.4 | 125.9 | 20.17 | $2.46\times10^3$ | 810.7 | 106.3 | 0.258 |
| AGN1 | 50±3 | 26±1 | − | 150 | 413.8 | 120.4 | 22.12 | $1.79\times10^3$ | 700.6 | 47.6 | 0.158 |
| AGN2 | 50±3 | 26±1 | − | 200 | 411.5 | 122.6 | 21.61 | $2.23\times10^3$ | 749.1 | 58.3 | 0.166 |

880 [a] Letters in abbreviations represent the reactants introduced into the chamber reactor, i.e., "G" represents
881 gasoline, "N" represents nitrogen oxides, "S" represents sulfur dioxide, "A" represents ammonia.
882 [b] The concentration of $NH_3$ is estimated by the amount of $NH_3$ added and the volume of the smog chamber.
883 [c] The surface area of aerosol particles measured by SMPS after 480 min of each experiment.
884 [d] SA yield was calculated after taking vapor and particle wall loss into account.

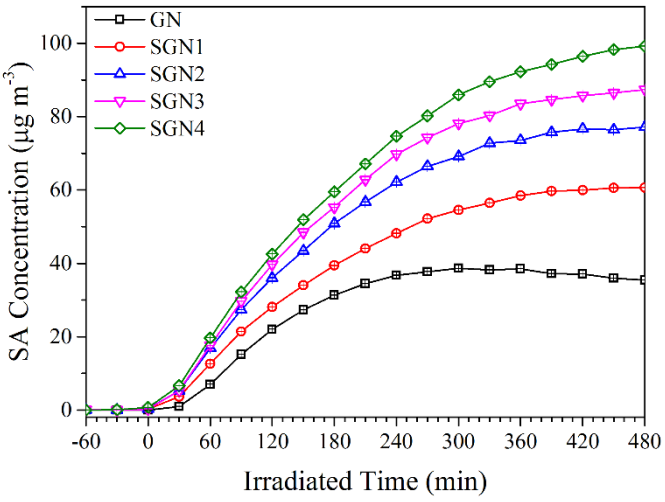


885

886 Fig. 1. Time series of secondary aerosol concentrations during the photo-oxidation experiments with different $SO_2$

887 concentrations (Exps. GN, SGN1, SGN2, SGN3, and SGN4).

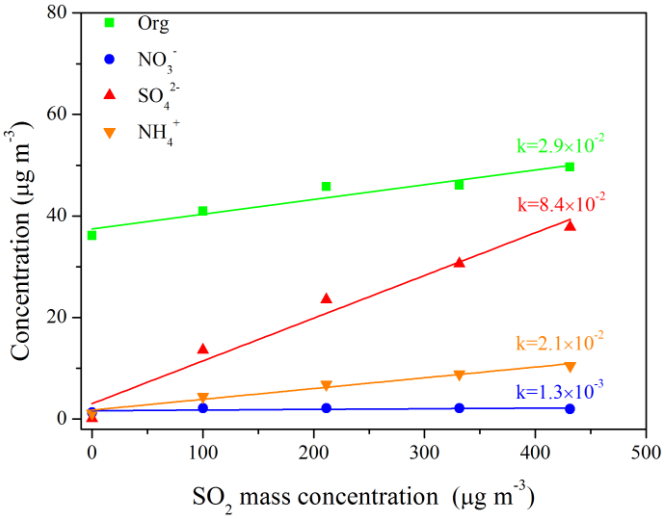


888

889 Fig. 2. Linear relationship between the concentration of chemical species (i.e., organic (green), nitrate (blue), sulfate (red), and

890 ammonium (orange)) and $SO_2$ under different $SO_2$ initial concentration conditions (Exps. GN, SGN1, SGN2, SGN3, and

891 SGN4). Each line represents a linear fitting and the k values are the corresponding slopes for each chemical species.

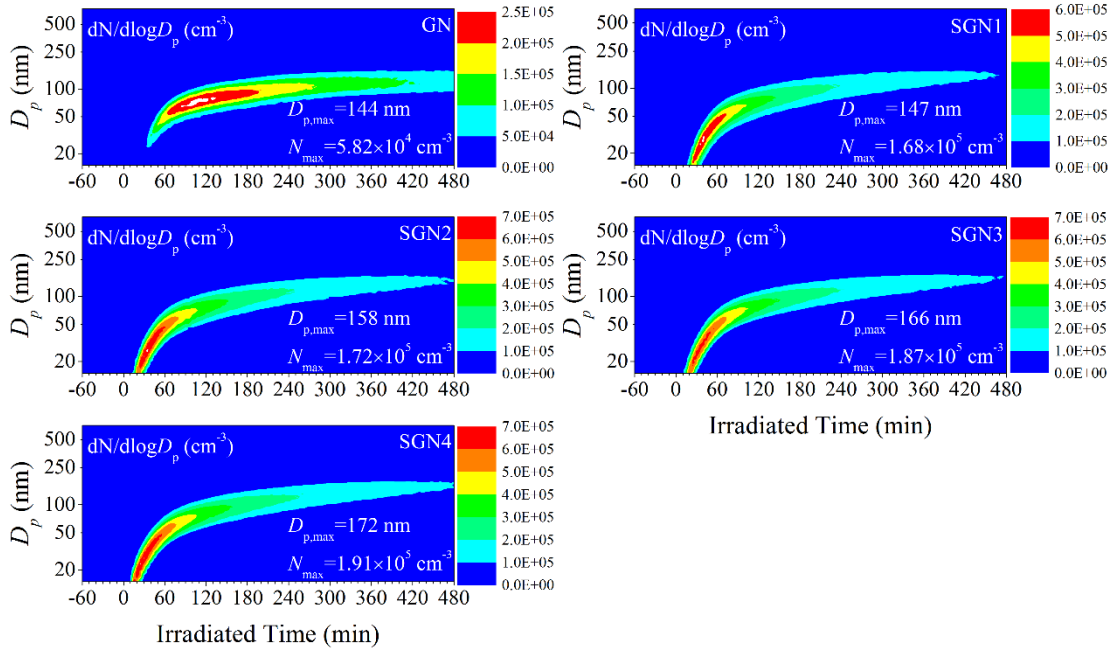


Fig. 3. Time series of the size distributions for the generated secondary aerosol during the photo-oxidation experiments with different $SO_2$ initial concentrations (Exps. GN, SGN1, SGN2, SGN3, and SGN4). $D_{p,max}$ and $N_{max}$ represent the maximal diameter and number concentration of generated secondary aerosol, respectively, during each photo-oxidation experiment.

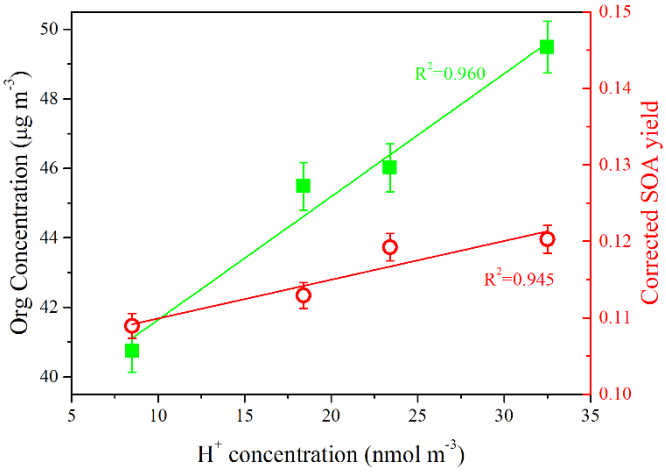


Fig. 4. Relationship between SOA concentration (left y axis), corrected SOA yield (right y axis) and $H^+$ concentration, which was used to characterize the particle acidities. The $H^+$ concentration presented in this plot was the value when the SOA formation rate reached the peak during each experiment (Exps. SGN1, SGN2, SGN3, and SGN4).

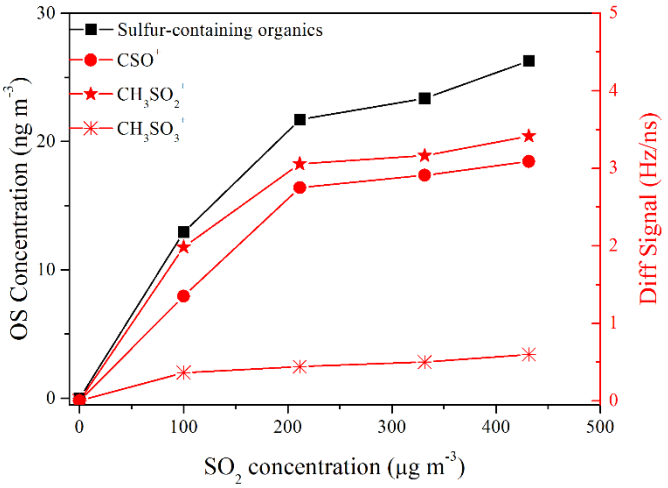


900

901 Fig. 5. Signal of fitted peaks, i.e., $CSO^+$, $CH_3SO_2^+$, $CH_3SO_3^+$ (right y axis) and sulfur-containing organics concentration (left

902 y axis) as a function of $SO_2$ initial concentration.

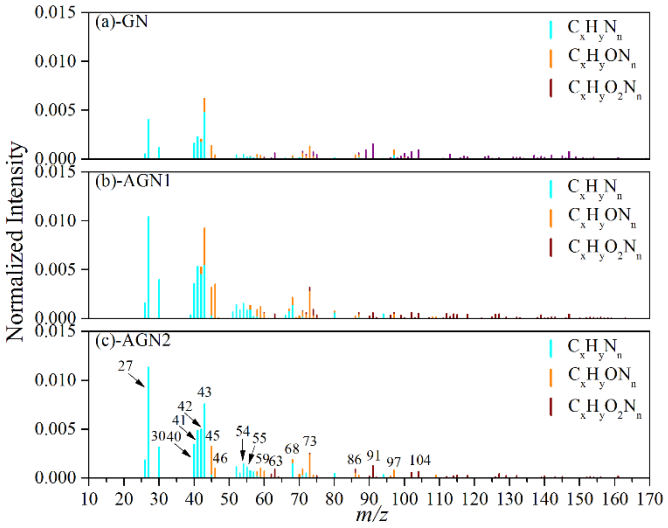


903

904 Fig. 6. Typical normalized mass spectra of N-containing fragments in SOA formed from the photo-oxidation of gasoline vapor

905 at different concentrations of $NH_3$ (Exps. GN, AGN1 and AGN2).

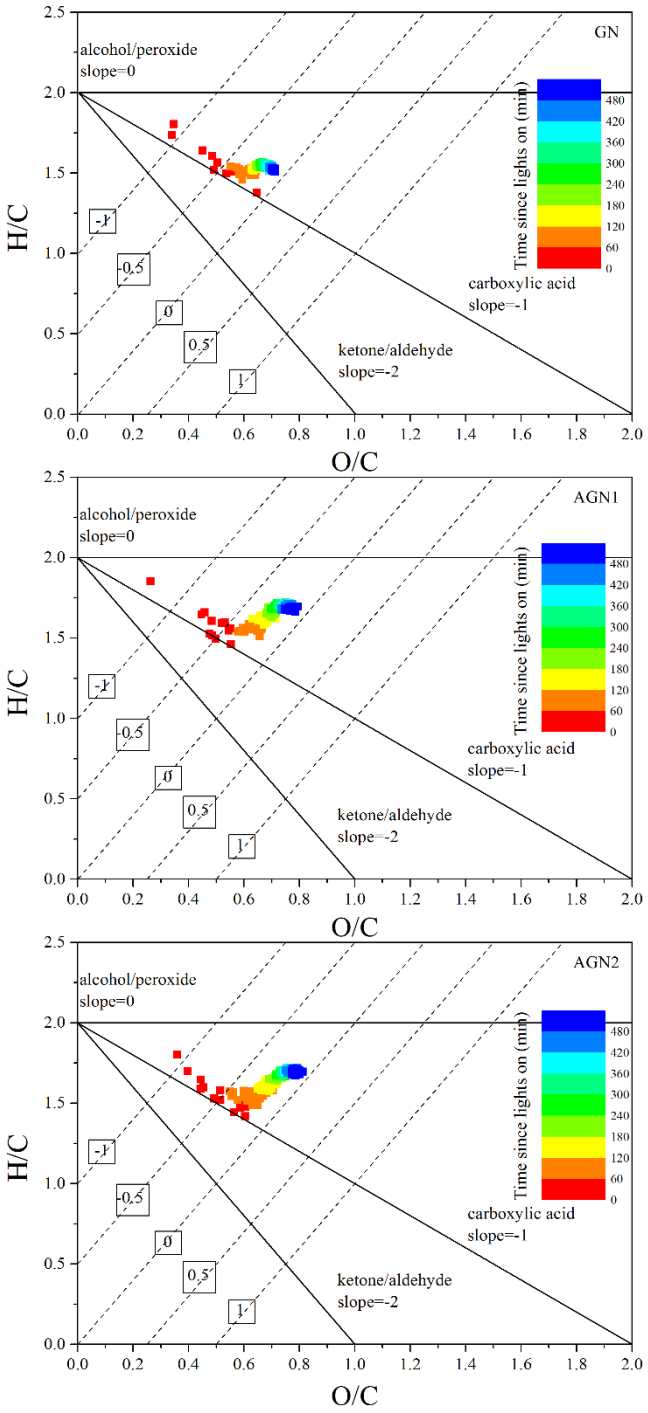


906

907 Fig. 7. Time evolution of H/C and O/C in SOA formed from the photo-oxidation of gasoline vapor at different concentrations

908 of $NH_3$ (Exp. GN, AGN1 and AGN2). The numbers (i.e., -1, -0.5, 0, 0.5, and 1) labeling the dashed lines show the average

909 carbon oxidation state (OSc $=$ 2×O/C−H/C) (Kroll et al., 2011). The black lines represent the addition of functional groups

910 to an aliphatic carbon (Heald et al., 2010).

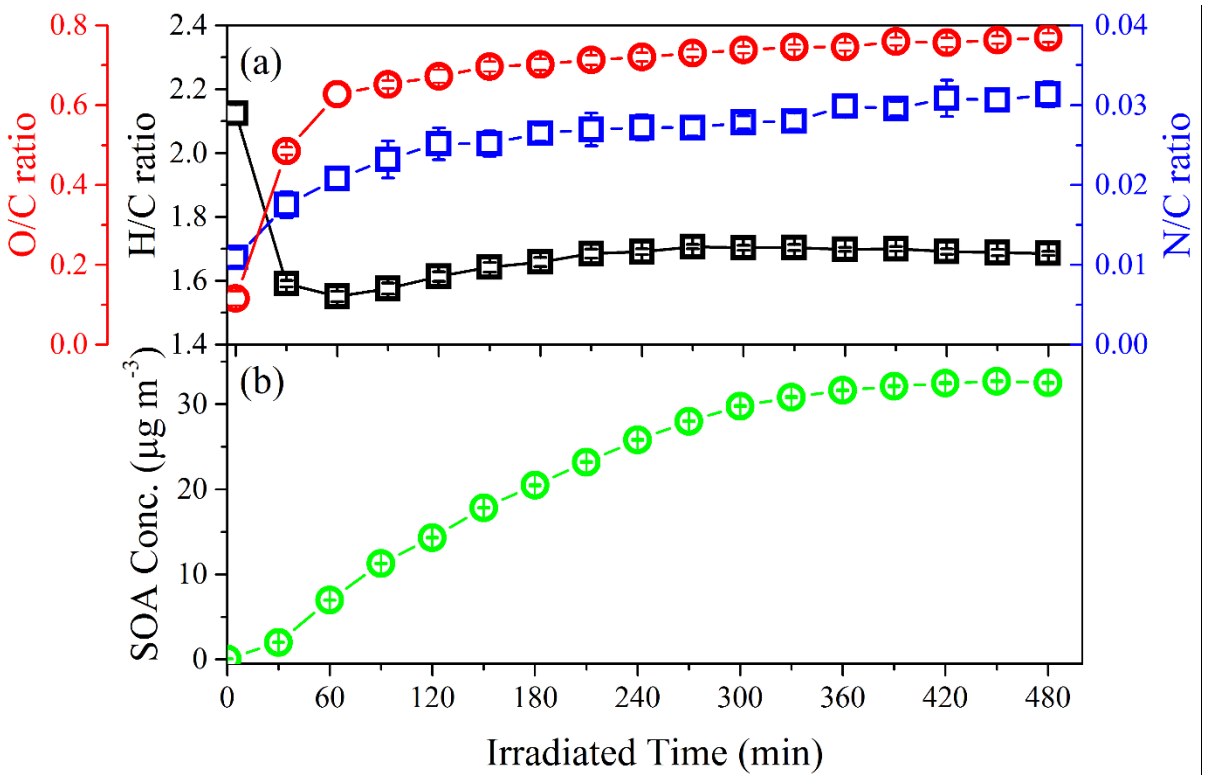


911

912 Fig. 8. Time evolution of (a) O/C, H/C and N/C and (b) SOA concentration in the photo-oxidation of gasoline vapor in the

913 presence of 150 ppb $NH_3$ (Exp. AGN1).

914

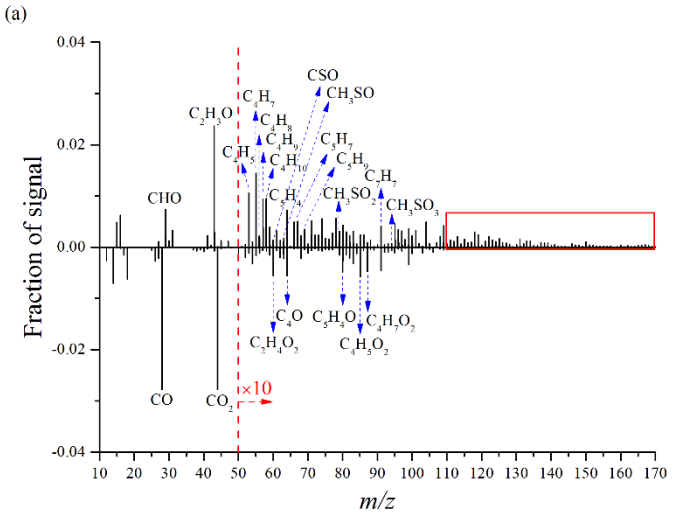


915

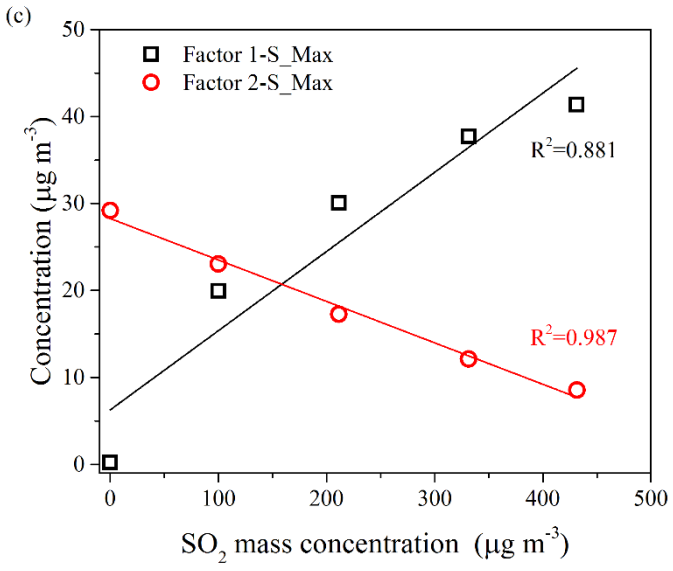


916

917 Fig. 9. (a) Difference mass spectra (Factor 1-S−Factor 2-S) between the two factors, (b) Time series of the mass concentration,

918 and (c) Relationship between the concentration of $SO_2$ and the maximum concentration of the two factors identified by

919 applying PMF analysis to the AMS data derived from the experiments at different concentrations of $SO_2$ (Exps. GN, SGN1,

920 SGN2, SGN3 and SGN4).

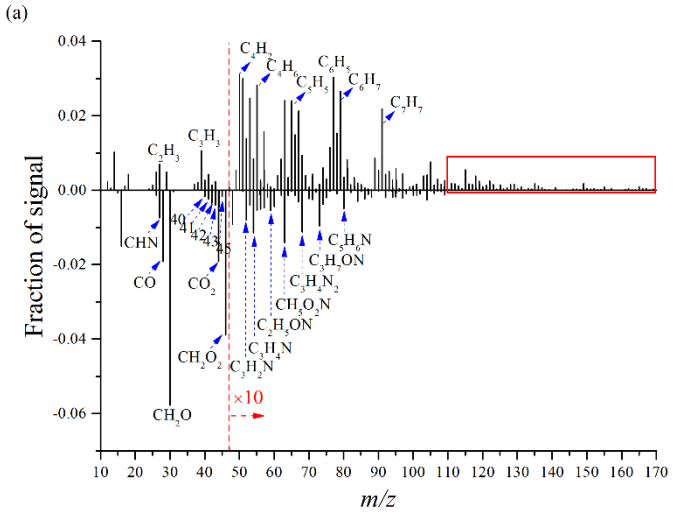


921

922

923

924 Fig. 10. (a) Difference mass spectra (Factor 1-N−Factor 2-N) between the two factors, (b) Time series of the mass

925 concentration, and (c) Relationship between the concentration of $NH_3$ and the maximum concentration of the two

926 factors identified by applying PMF analysis to the AMS data derived from the experiments at different

927 concentrations of $NH_3$ (Exps. GN, AGN1 and AGN2).